Instituto Alberto Luiz Coimbra de
Pós-Graduação e Pesquisa de Engenharia

BEHAVIOUR AND DSM DESIGN OF COLD-FORMED STEEL WEB/FLANGE STIFFENED LIPPED CHANNEL COLUMNS EXPERIENCING DISTORTIONAL FAILURE

Rafaela Alves Sanches Garcia

Dissertação de Mestrado apresentada ao Programa de Pós-graduação em Engenharia Civil, COPPE, da Universidade Federal do Rio de Janeiro, como parte dos requisitos necessários à obtenção do título de Mestre em Engenharia Civil.

Orientadores: Alexandre Landesmann
Dinar Reis Zamith Camotim

Rio de Janeiro
Março de 2015

BEHAVIOUR AND DSM DESIGN OF COLD-FORMED STEEL WEB/FLANGE STIFFENED LIPPED CHANNEL COLUMNS EXPERIENCING DISTORTIONAL FAILURE

Rafaela Alves Sanches Garcia

DISSERTAÇÃO SUBMETIDA AO CORPO DOCENTE DO INSTITUTO ALBERTO LUIZ COIMBRA DE PÓS-GRADUAÇÃO E PESQUISA DE ENGENHARIA (COPPE) DA UNIVERSIDADE FEDERAL DO RIO DE JANEIRO COMO PARTE DOS REQUISITOS NECESSÁRIOS PARA A OBTENÇÃO DO GRAU DE MESTRE EM CIÊNCIAS EM ENGENHARIA CIVIL.

Examinada por:

Prof. Alexandre Landesmann, D.Sc.

Prof. Eduardo de Miranda Batista, D.Sc.

Prof. Luciano Rodrigues Ornelas de Lima, D.Sc.

RIO DE JANEIRO, RJ – BRASIL

MARÇO DE 2015

Garcia, Rafaela Alves Sanches

Behaviour and DSM design of cold-formed steel web/flange stiffened lipped channel columns experiencing distortional failure / Rafaela Alves Sanches Garcia. – Rio de Janeiro: UFRJ/COPPE, 2015.

VIII, 73 p.: il.; 29,7 cm.

Orientadores: Alexandre Landesmann

Dinar Reis Zamith Camotim

Dissertação (mestrado) – UFRJ/ COPPE/ Programa de Engenharia Civil, 2015.

Referências Bibliográficas: p. 63-66.

1. Distortional failure. 2. Cold-formed steel columns. 3. Numerical analysis. I. Landesmann, Alexandre *et al*. II. Universidade Federal do Rio de Janeiro, COPPE, Programa de Engenharia Civil. III. Título.

ACKNOWLEDGEMENTS

To all my family, for the good thoughts. Especial thanks to my parents, my sister and my husband for all understanding and love. Thank you for all support and for standing by my side during all this time encouraging me to go on and to follow my dreams. Without you this journey would be much more difficult.

To my friends from COPPE, for bringing hope in hard moments and for being the best friends I could imagine. Thank you for all happy and funny moments that we lived together. You will always be in my heart.

To my friends from INUSA, for the first opportunity to work with steel structures. Undoubtedly, this was a cornerstone in my life. Thank you for sharing so much knowledge and for being present in my life after these years.

To my advisors, Prof. Alexandre and Prof. Camotim, thank you for all the knowledge shared, support, advising and friendship. It was a pleasure to be instructed by you in this work and I am eternal grateful for all your support.

To my colleagues from Department of Graphic Expression/UFRJ, especially to Profª Paula and Profª Gabriella, for helping me with my first experience as a teacher. Thank you for your support and advices about teaching. It was rewarding to work with you during this period.

To COPPE, for providing the opportunity to produce this work.

To CNPq, for the financial support.

Resumo da Dissertação apresentada à COPPE/UFRJ como parte dos requisitos necessários para a obtenção do grau de Mestre em Ciências (M.Sc.)

COMPORTAMENTO E DIMENSIONAMENTO VIA MRD DE COLUNAS DE AÇO EM PERFIL FORMADO A FRIO COM ENRIJECEDORES NA ALMA E NAS MESAS SOB O MODO DE FALHA DISTORCIONAL

Rafaela Alves Sanches Garcia

Março/2015

Orientadores: Alexandre Landesmann
Dinar Reis Zamith Camotim
Programa: Engenharia Civil

Resultados recentemente relatados por KUMAR & KALYANARAMAN (2014) sugerem que a presença de enrijecedores intermediários em "V" na alma e nas mesas de colunas U_e em perfil formado a frio pode alterar consideravelmente o comportamento de flambagem, pós-flambagem e colapso das colunas. Em particular, isso pode implicar que o Método da Resistência Direta (MRD) tenha uma curva de dimensionamento diferente para colunas com enrijecedores na alma e mesas. O objetivo deste trabalho é avaliar a validade desta afirmação, a qual representa um quebra significativa do conhecimento existente amplamente aceito pela comunidade científica. Este trabalho relata uma investigação numérica destinada à análise do comportamento de flambagem distorcional, pós-flambagem e colapso de colunas U_e com enrijecedores na alma e mesas e U_e planas que compartilham características mecânicas similares. A primeira etapa consiste da seleção da geometria das colunas com flambagem e falha "puramente" distorcional. Em seguida, é abordada a caracterização mecânica dos modos de flambagem distorcional em colunas enrijecidas, o que não é tão óbvio quanto em colunas planas. Então, um modelo em elementos finitos no ANSYS é empregado para análise não-linear geométrica e material. Os resultados numéricos obtidos são apresentados, discutidos e comparados. Finalmente, tomando os resultados de resistência última obtidos e dados coletados da literatura, o trabalho apresenta algumas considerações a respeito da atual curva MRD para o dimensionamento de colunas com enrijecedores intermediários sob modo de falha distorcional.

Abstract of Thesis presented to COPPE/UFRJ as a partial fulfillment of the requirements for the degree of Master of Science (M.Sc.)

BEHAVIOUR AND DSM DESIGN OF COLD-FORMED STEEL WEB/FLANGE STIFFENED LIPPED CHANNEL COLUMNS EXPERIENCING DISTORTIONAL FAILURE

Rafaela Alves Sanches Garcia

March/2015

Advisors: Alexandre Landesmann
Dinar Reis Zamith Camotim
Department: Civil Engineering

Results recently reported by KUMAR & KALYANARAMAN (2014) suggest that the presence of web and flange V-shaped intermediate stiffeners in cold-formed steel lipped channel columns may considerably alter their distortional buckling, post-buckling and collapse behaviours. In particular, it may even imply that the application of the Direct Strength Method (DSM) to web/flange-stiffened lipped channel columns requires the consideration of a different distortional strength curve. The objective of this work is to asses the validity of this assertion, which constitutes a significant break from existing knowledge, which is widely accepted by the scientific community. This work reports a numerical investigation addressed to the distortional buckling, post-buckling and collapse behaviours of (web/flange) stiffened and plain cold-formed steel lipped channel columns sharing similar mechanical features. The first step consists of selecting column geometries associated with "pure" distortional buckling and failure modes. Then, it is necessary to address the mechanical characterization of the distortional buckling modes in the stiffened columns, which is not so obvious than in the plain columns. Next, an ANSYS shell finite element model is employed to perform geometrically and materially non-linear analysis. The numerical results obtained are then presented, discussed and compared. Finally, on the basis of the ultimate strength data obtained and experimental failure loads collected from the literature the work presents some considerations concerning the current DSM strength curve to design (web/flange) stiffened lipped channel columns failing in distortional modes.

INDEX

SYMBOLS

Roman letters

A	cross-section area
E	modulus of elasticity
f_y	yield stress
I	inertia
L	member length
L_D	member length associated to distortional buckling
P	axial compression load
$P_{b1.L}$	lowest local bifurcation load
$P_{b1.G}$	lowest global bifurcation load
P_{cr}	critical load (or bifurcation load)
$P_{cr.D}$	distortional buckling critical load
P_E	*Euler* critical load
$P_{n.D}$	nominal member capacity in distortional buckling
P_u	ultimate strength
P_y	squash load ($P_y = Af_y$)

Greek letters

δ	column transversal deflection
δ_a	column axial shortening
δ_0	initial imperfection
λ	slenderness
λ_D	slenderness associated to distortional buckling
λ_L	slenderness associated to local buckling
ν	Poisson's ratio

1 Introduction

Cold formed steel (CFS) members are composed by elements with large width-to-thickness ratios (slender-element members). It is produced by bending a thin plate of steel, at room temperature, into a shape that supports more load than the sheet itself. Basically, there are two processes to manufacture a cold-formed member: roll forming and brake forming. The first one (Figure 1.1(a)) consists of a pair of opposing rolls, fed by a continuous steel strip, that progressively deform the steel to obtain the desired shape. Each pair of rolls yields a limited amount of deformation. The second process (Figure 1.1(b)) uses a press brake machine that produces one complete fold at time along the length of the member. The thin plate can be bended in several geometries. Some examples of the most common CFS cross-sections are indicated in Figure 1.2.

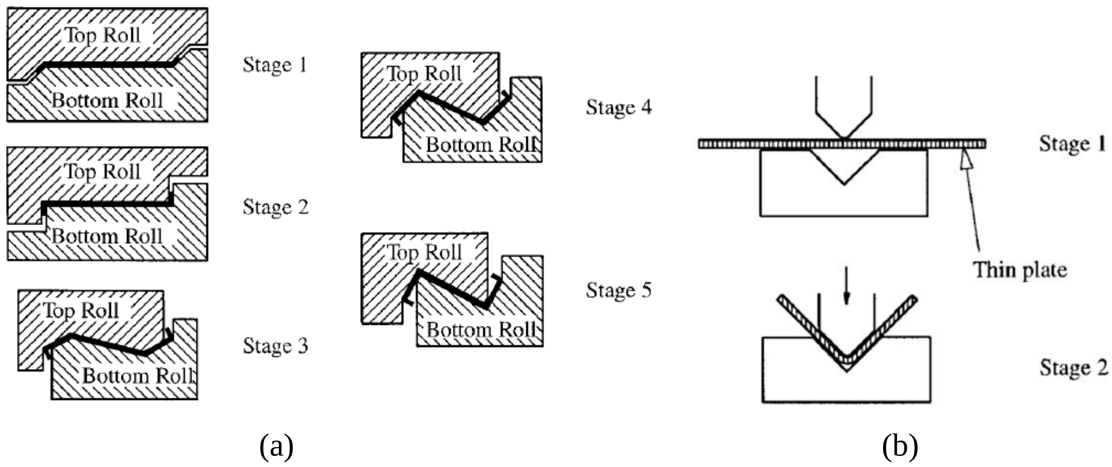

Figure 1.1. Cold forming processes: (a) roll forming; (b) brake forming (HANCOCK *et al.,* 2001).

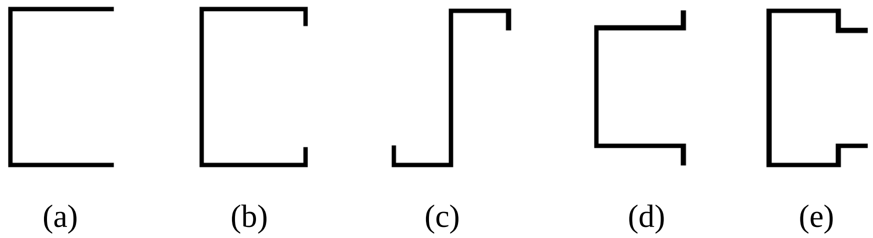

Figure 1.2. Examples of most common CFS cross-sections: (a) plain channel, (b) plain lipped channel, (c) *Z* lipped section, (d) hat and (e) rack.

CFS members are widely used in light-weight structures, for instance warehouses, mezzanines, residential framing, storage racks and small buildings (Figure 1.3(a-c)). Its use has been increasing due to reduced manufacturing time and costs, and agility in the building process demanded by the market of construction.

In comparison to other materials, for example concrete or welded steel structures, CFS members present some advantages. It is more versatile in construction and assembly of several types of structures, the quality control is easier, it does not require skilled labor and it can be manufactured in several different cross-section shapes. Thus, it is very adaptable making possible its use together with another constructive system (Figure 1.3(d)). In addition, due to its light weight, handling, erection and transporting of CFS members is relatively easy.

(a)

(b)

(c)

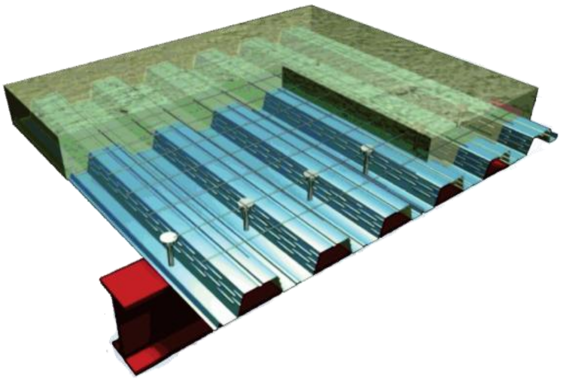

(d)

Figure 1.3. Examples of CFS application: (a) residence in light steel framing system (CSSBI, 2014), (b) storage structure (DNA NACIONAL, 2014), (c) small buildings (CSSBI, 2014) and (d) steel deck with concrete slab (METFORM, 2014).

1.1 Historic

Although the use of light steel structures started in both United States and England around 1850 its use was limited to basic structures. Despite requirements for hot-rolled steel had already been adopted into building standards in the 1930's, there were no provisions for cold-formed steel. Thus, the acceptance of CFS as a construction material was still limited. In 1933, during the World’s Fair in Chicago, a completely steel framed house prototype was featured (Figure 1.4). Also, in this fair, the first standing seam metal roofing panel was displayed, indicating a strong tendency of using this material.

Due to The Second World War, the steel building industry began to grow, triggering the improvement of manufacturing processes. In 1939, the American Iron and Steel Institute (AISI) realized that a standard for cold-formed steel was necessary. Hence, the first specification for designing of light steel structural members was published in 1946 by AISI due to researches carried out by George Winter, at Cornell University. (DON ALLEN, 2006).

Figure 1.4. Prototype of steel framed residence (DON ALLEN, 2006).

In Brazil, before 1990 the design of CFS members was based on foreign specifications even though this material was already used in construction (BATISTA & GHAVAMI, 2005). Thus, in order to keep updated about the new design methods developed by engineering researches, the Brazilian standard for cold-formed structural members (ABNT, 2010) were recently reviewed allowing appropriate design using new steel structural solutions.

Advances in the manufacturing process have triggered the cold-formed steel industry to search for novel cross-section shapes that, in comparison to the most traditional ones, are structurally more efficient (they exhibit higher strength-to-weight ratios). This efficiency is commonly achieved by including more or less complex intermediate or edge stiffeners. Typical forms of intermediate and edge stiffeners for CFS members are shown in Figure 1.5(a) and 1.5(b), respectively. This trend was responsible for (i) the emergence of distortional failures (poorly understood two decades ago) and (ii) the inadequacy of the method classically adopted to handle local failures, the widely accepted Effective Width Method (EWM) – its application to more complex cross-section shapes (see Figure 1.6) involves tiresome and time-consuming calculations.

(a) (b)

Figure 1.5. Typical (a) intermediate and (b) edge stiffeners (EUROCODE 3, 1993).

In order to overcome the difficulties of the EWM, SCHAFER & PEKÖZ (1998) proposed the Direct Strength Method (DSM), which has its roots in the work of HANCOCK *et al.* (1994) and mainly owes its progressive development, dissemination and establishment amongst the cold-formed steel technical community to the efforts of SCHAFER (2000, 2002, 2008). Due to its simplicity and efficiency the DSM has become increasingly popular worldwide. In fact, it has already included in the current versions of the North American (AISI, 2012), Australian/New Zealand (AS/NZS, 2005) and Brazilian (ABNT, 2010) specifications for cold-formed steel structures.

Figure 1.6. Examples of CFS complex cross-section geometry (ENCON, 2015).

1.2 Motivation

Although CFS has been largely used in construction it is highly susceptible to instability phenomena. The current DSM provides design curves/expressions to estimate the load-carrying capacity of members failing in local, distortional, global and local-global interactive modes.

For columns design, the DSM curves were calibrated and validated against numerical and experimental failure loads concerning almost exclusively members with fixed-ended support conditions[1] and, most of them, exhibiting plain cross-section shapes (without intermediate stiffeners). Thus, the DSM application to columns with other characteristics has raised some doubts. For instance, (i) extensive parametric studies reported by LANDESMANN & CAMOTIM (2011, 2013) showed that the current DSM distortional strength curve overestimates the failure loads of plain columns with other end support conditions and (ii) an experimental and numerical investigation reported by KUMAR & KALYANARAMAN (2014) suggested that the curve underestimates the failure loads of fixed-ended lipped channel columns with web and flange V-shaped intermediate stiffeners (see Figure 1.5(a)). It worth mention that this specific cross-section was not considered in the calibration/validation studies to propose the current DSM.

Despite the fact there is a remarkable number of numerical analysis of CFS members reported in literature, only a small fraction of these studies addresses lipped channel columns with intermediate stiffeners in web and flanges under distortional buckling and failure. Such studies are basically the work done by SILVESTRE *et al.* (2005), SILVESTRE & CAMOTIM (2006), GARCIA *et al.* (2014) and KUMAR & KALYANARAMAN (2014). The conclusions and suggestions drawn by the authors of this last publication constitute a significant break from the existing knowledge, providing the motivation for the investigation reported in this thesis.

---

[1] The calibration and validation of the DSM distortional design curve/expressions involved almost exclusively columns with rigid plates attached to their end cross-sections. Although SCHAFER (2000) mentions that the pined-pined condition were tested, this statement is related to the column global behavior (the rigid plates usually rest on spherical hinges, knife edges or weges) – as far as the distortional behavior is concerned, the columns are fixed.

1.3 Objective

The objective of this work is to present and discuss results of a numerical investigation concerning “pure” distortional buckling, post-buckling and collapse behavior of cold-formed steel lipped channel columns with web and flange V-shaped intermediate stiffener and plain lipped channel columns (henceforth designated as SLC and PLC, respectively) sharing similar mechanical features. The use of the word “pure” means that there is no influence from either local or global buckling/deformations, which is ensured by selecting columns with local and global critical buckling loads significantly higher than their distortional counterparts. In particular, it is intended to verify the assertions made by KUMAR & KALYANARAMAN (2014). At first, it is believed there is no need to develop a new DSM distortional design curve for fixed-ended SLC columns.

As part of the main objective the following results are achieved: (i) buckling modal participation through GBTUL, (ii) evaluation of elastic and elastic-plastic post-buckling, (iii) evaluation of ultimate strength, P_u /P_y *vs.* λ_D curves, obtained from the ANSYS and compared with Direct Strength Method (DSM), and (iv) a comparison of the results together with data collected from the literature.

1.4 Outline

Initially, in Chapter 2, a bibliography review is presented relating previous works addressed to buckling and post-buckling behaviour of CFS members under centered compression by numerical and experimental analysis and design methods.

Next, Chapter 3 describes the column selection procedure, which aims at identifying SLC and PLC column geometries (cross-section dimensions and lengths) that ensure (i) buckling in pure distortional modes and (ii) local and global critical buckling loads significantly higher than their distortional counterparts. In order to clarify the distinction between local and distortional buckling in SLC (unlike in the PLC columns, this distinction is not straightforward in SLC), the column selection procedure is followed by the presentation and discussion of SLC column buckling results obtained through analysis based on Generalized Beam Theory (GBT), whose modal nature makes it possible to illustrate and clarify the meanings of the words “local” and “distortional” adopted in this work.

Then, after describing the ANSYS (SAS, 2009) shell finite element model adopted, Chapter 4 presents the validation step and some considerations concerning the work done by KUMAR & KALYANARAMAN (2014). A set of *5* columns previously analyzed by KUMAR & KALYANARAMAN were chosen for the validation step in order to verify whether the model idealized in this work is adequate.

Chapter 5 addresses the elastic distortional post-buckling behaviour of the selected columns, focusing on the differences between SLC and PLC columns in order to assess the influence of the intermediate stiffeners. It is also presented the elastic-plastic post-buckling behaviour, the ultimate strength obtained through ANSYS and the DSM. The numerical results presented and discussed comprise equilibrium paths, failure loads and deformed configurations, including the collapse mechanisms. The failure loads gathered in this work, together with additional ultimate strength data (numerical and experimental) collected from the literature, assess the merits of the current DSM distortional design curve, namely its applicability to SLC columns, which was challenged by KUMAR & KALYANARAMAN (2014).

Finally, the main conclusions and suggestions for future work are presented in Chapter 6.

2 Bibliography Review

Item 2.1 presents stability and equilibrium concepts, focusing on the buckling modes and the main previous works concerning to distortional buckling, post-buckling behaviour, and ultimate strength. The design methods and standards are addressed in item 2.2.

2.1 Structural stability and equilibrium

Structural design must consider not only safety and strength requirements but also stability requirements (especially for slender members). Considering a structure under external forces presenting a specific equilibrium configuration, the stability of this configuration is assessed through the structural behaviour after a slight perturbation caused by a little external force. The equilibrium is stable or unstable whether the structure returns or not to its original position after the perturbation had finished. (REIS & CAMOTIM, 2001). As for columns, the stability concept is exemplified by a classical problem: the *Euler column*. This cornerstone of column theory consists in (i) an elastic column, (ii) perfectly straight, (iii) with length *L*, (iv) with simple supported ends and (v) axially loaded (*P*) (see Figure 2.1(a)). Its equilibrium path, which is the lateral displacement (*q*) at mid-length *vs.* load, is presented in Figure 2.1(b).

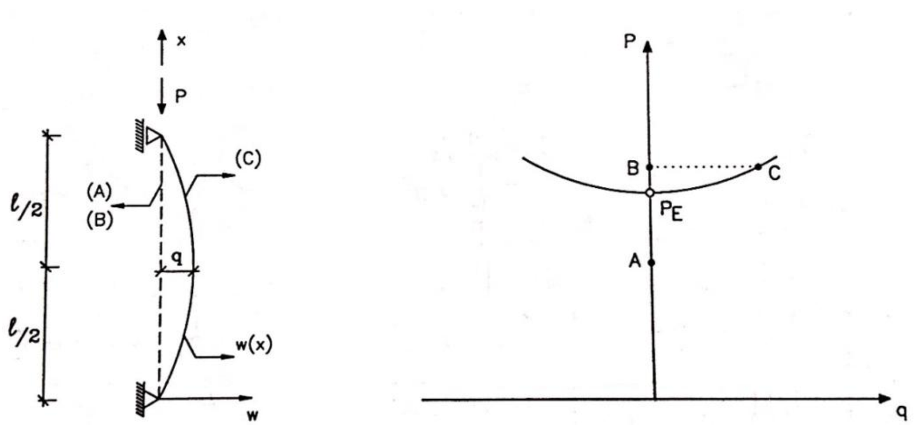

(a) (b)

Figure 2.1. *Euler column*: (a) geometry and load and (b) equilibrium path (REIS & CAMOTIM, 2001).

In Figure 2.1(b), the region where $q=0$ and $q\neq 0$ are named as "fundamental path" and "post-buckling path"[2], respectively. The intersection of these two paths is designated as *Euler critical load* (P_E), or bifurcation load, and it can be evaluated by Equation 2.1. The critical load provokes a bifurcation in the equilibrium configuration – the column can remain straight or it can present any displacement. The deflected shape is given by Equation 2.2.

$$P_E = \frac{\pi^2 EI}{L^2} \qquad \text{(Eq. 2.1)}$$

$$w(x) = q.sen\frac{\pi x}{L} \qquad \text{(Eq. 2.2)}$$

Still considering the equilibrium path indicated in Figure 2.1(b), the points A, B and C represent three different configuration of the column (B and C correspond the same load). After a slight perturbation, due to a little force δF, in point A ($P<P_E$ and $q=0$, Figure 2.2(a)) the column regresses to its original position. Thus, this is a stable equilibrium. On the other hand, in point B ($P>P_E$ and $q=0$, Figure 2.2(b)) the column "moves away" from its original position, presenting an unstable equilibrium. Hence, this latter case leads the column to the equilibrium configuration C. If a new slight perturbation is introduced in C ($P>P_E$ and $q\neq 0$, Figure 2.2(c)), then it results a stable equilibrium[3]. In fact, the critical load marks the transition from stable to unstable equilibrium. The *Euler load* represents the smallest load that causes a change in the equilibrium state of the idealized column. (IYENGAR, 1986)

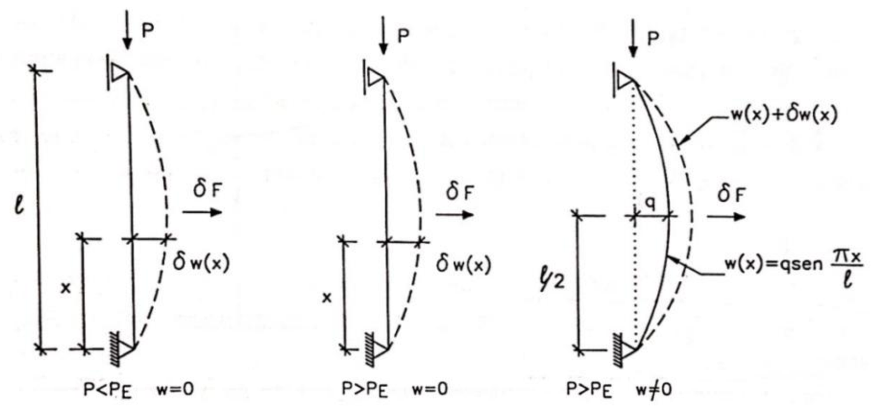

(a) (b) (c)

Figure 2.2. *Euler Column* equilibrium configurations (a) stable equilibrium, (b) unstable equilibrium and (c) stable equilibrium (REIS & CAMOTIM, 2001).

[2] More details about buckling and post-buckling will be presented in the next section.
[3] Additional information about structural instability can be found in REIS & CAMOTIM (2001).

2.1.1 Buckling, post-buckling and ultimate strength

When a steel member is submitted to a load, higher than its critical load, it loses its original shape somehow. This effect is called *buckling* and it will be addressed next for columns under centered compression load.

a) Buckling

Buckling is the loss of the original shape of a member as a result of elastic or inelastic strain (ZIEMIAN, 2010). This change in the shape might be named as local, distortional or global (flexural or flexural-torsional) buckling. Depending on the member features anyone of these buckling modes can be the associated to the critical load.

Local buckling involves plate flexure alone without transverse deformation and line junctions between elements remain straight. *Distortional buckling* involves changing in cross-sectional shape excluding local buckling (HANCOCK, 2003). Also, it presents rotation at the web-flange junction in typical members (SCHAFER, 2000). *Global buckling* holds two buckling shapes: (i) *flexural buckling* results from a bend in compression members without change of cross-sectional shape and (ii) *flexural-torsional buckling (or torsional)* involves bend and twist simultaneously without change of cross-sectional shape as well. The shortening that occurs in a compression member is type as global buckling. For better understanding on how these buckling shapes are, Figure 2.3 shows some of the main in-plane buckling shapes for an arbitrary plain lipped channel column.

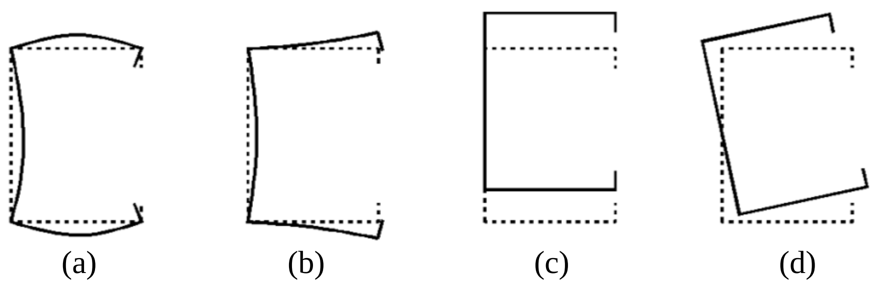

Figure 2.3. In-plane buckling shapes for plain lipped channel column: (a) local, (b) distortional, (c) flexural (major axis bending) and (d) torsional buckling.

Based on the Generalized Beam Theory (GBT) the software GBTUL (BEBIANO *et al.* 2008, 2010a,b) is a very effective tool to perform buckling analysis[4]. This freeware program requires the mechanical features and cross-section dimensions of the member as input and provides, among other results, (i) in-plane deformation of buckling modes, (ii) signature curve and (iii) participation of each one of buckling modes cited above.

The GBTUL cross-section analysis yields a set of N_d deformation modes (Equation 2.3), which represent the possible cross-section deformation patterns to be accounted for (BEBIANO *et al.* 2010a). The quantity of deformation modes depends on the number of walls (n) and the number of intermediate nodes (m). Figure 2.4(a) indicates natural and intermediate nodes as red and yellow marks, respectively. The extremity nodes are always treated as both natural and intermediate nodes (green marks).

$$N_d = n + 1 + m \qquad \text{(Eq. 2.3)}$$

Figure 2.4(b) shows the first *13* in-plane deformation modes for an arbitrary plain lipped channel: (i) the first *4* are the rigid-body *global* modes – axial extension (mode **1**), major and minor axis bending (modes **2** and **3**) and torsion (mode **4**), (ii) modes **5** and **6** are distortional and (iii) the remaining are local-plate modes, which involve exclusively wall bending (their number is equal to the number of intermediate modes considered, *m*). Depending on the geometry (cross-section dimensions and length) and support conditions, any of these buckling modes may be the critical one. It is worth to mention that only sections with at least 4 walls have distortional modes.

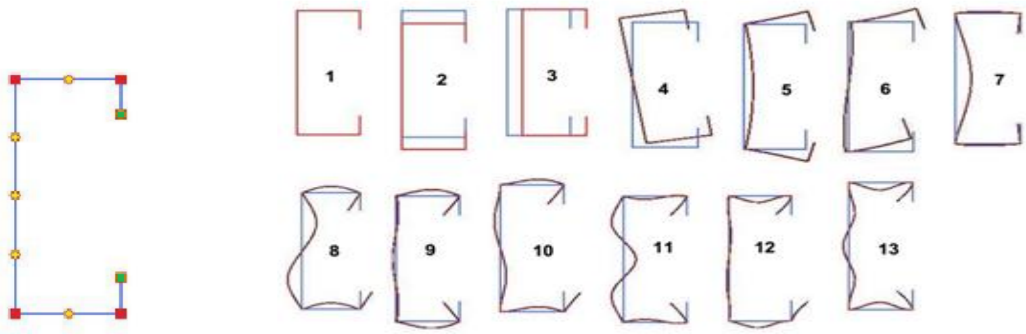

(a) (b)

Figure 2.4. Cross-sections analyses in GBTUL (a) nodal discretization and (b) in-plane deformed configuration of plain lipped channel column (BEBIANO *et al.*, 2010a).

[4] GBTUL also provides tools for vibration analysis of elastic thin-walled members, this is not the goal of this thesis though.

Another result of buckling analysis performed on GBTUL is the signature curve (which relates the member length and its critical load). For columns simply-supported, the "minimum" at the signature curve corresponds to critical loads that lead to local or distortional buckling. Figure 2.5 exemplifies this curve for a plain lipped channel and indicates the buckling shape for each critical load.

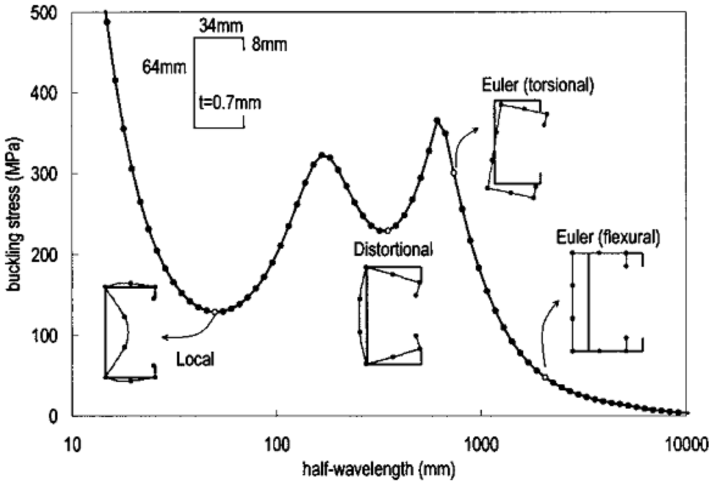

Figure 2.5. Example of signature curve for simply supported plain lipped channel column (SCHAFER, 2002).

For columns with fixed-ended support conditions this curve is quite different. Unlike simply-supported columns (Figure 2.6(a)), the signature curve of fixed-ended columns does not present minimum (Figure 2.6(b)). Thus, in order to evaluate the buckling mode of the member is crucial to assess the modal participation.

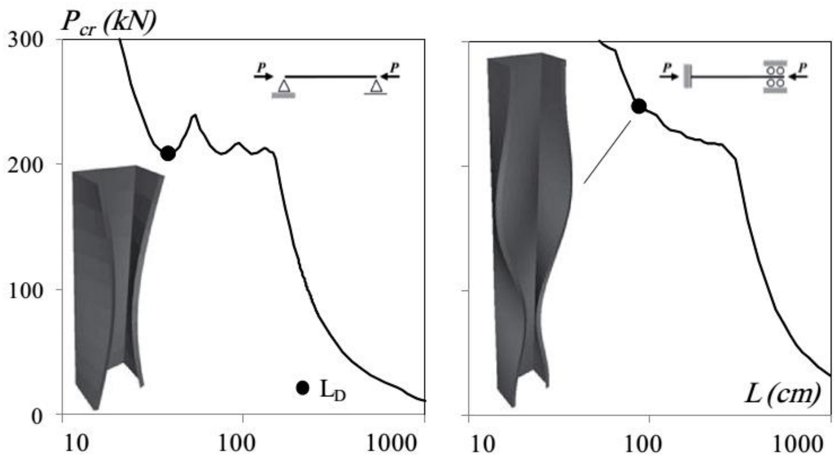

Figure 2.6. Signature curve for (a) simply-supported and (b) fixed-supported columns distortionally buckled (LANDESMANN & CAMOTIM, 2013).

Indeed, the buckling shape consists in a combination of the existing buckling modes. This means, even if a column clearly buckles in a distortional shape, it might exists some participation of the others buckling modes. Thus, for classification of buckling - in local, distortional or global one - it must be considered the percentage of participation of each buckling mode[5]. Figure 2.7 shows an example of GBT modal decomposition of a plain lipped channel distortionally buckled.

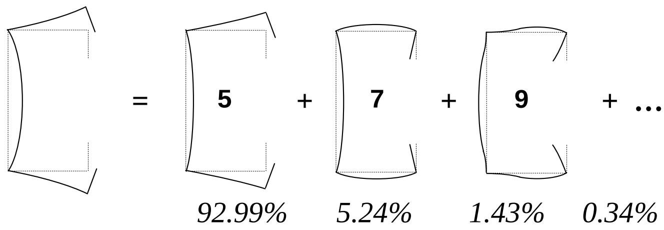

Figure 2.7. Illustrative GBT modal decomposition: distortionally buckled mid-span PLC column (LANDESMANN *et al.*, 2013).

Among other results, LANDESMANN *et al.* (2013) concluded that there are clear correlation between modal participation and the *web/flange* width ratio. Figure 2.8 plots the participation of modes **5** (***p_5***), **7** (***p_7***) and **9** (***p_9***) (GBTUL numbering) against the *web/flange* ratio for PLC column. It is observed that ***p_5*** decreases as *web/flange* ratio increases. At the same time ***p_7*** increases as well, probably due to the higher vulnerability of wider webs to local deformations. Conversely, no tendency is detected in ***p_9*** plots.

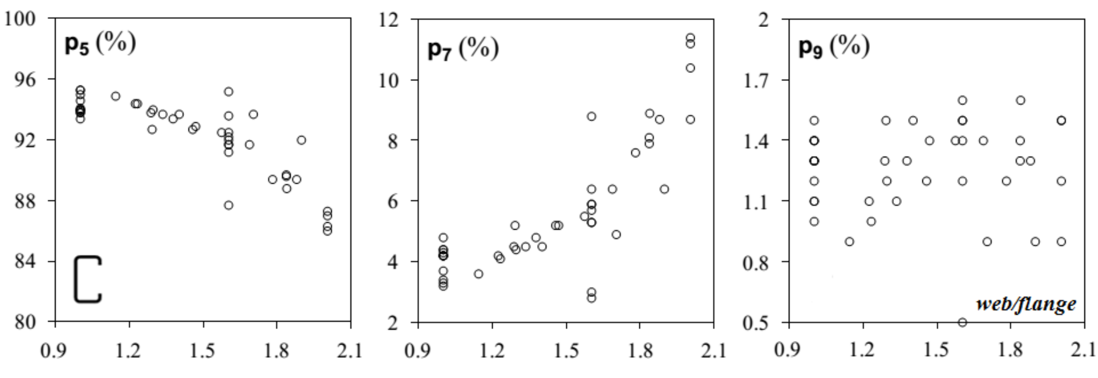

Figure 2.8. Variation of ***p_5***, ***p_7*** and ***p_9*** with *web/flange* ratio (LANDESMANN *et al.*, 2013).

In general, one buckling mode is noticeable prevalent. However, depending on the member features a modal interaction may occur, which means that more than one

[5] Usually, the buckling mode with participation higher than *80%* is considered the main one but this is not set in stone. The whole behavior of the member has to be observed.

buckling mode is relevant for the column behaviour. Some works have addressed this specific situation (*e.g.* DINIS & CAMOTIM 2010, SANTOS *et al*. 2012 and DINIS *et al.* 2014), this subject is not the goal of this thesis though.

The software ANSYS is also a good tool for buckling analysis and some works have already proved that it is accurate for critical load prediction (*e.g.* SILVESTRE & CAMOTIM 2006 and BASAGLIA *et al.* 2011). Results obtained through GBTUL and ANSYS are very similar, or even equal. However, it is not possible to obtain modal participation through ANSYS.

In most cases, the critical load of a compression member, obtained from the linear buckling analysis of a perfect member, is not the same load at which a real imperfect member collapses. Thus, it is necessary to assess the post-buckling behaviour.

b) Post-buckling and ultimate strength

Axially loaded columns initially shorten due to axial compression. Then, at the critical load, the column begins to buckle and its stiffness may either increases or decreases. Figure 2.9 shows an elastic equilibrium path (or load-deflection curve) where solid lines illustrate the behaviour of perfect members and dashed lines indicate the theoretical behaviour for the same member when a given degree of imperfection is assumed (δ_0). If the load supported by the structure after the onset buckling increases with increasing deformation, as shown in Figure 2.9(a), the structure has a *stable post-buckling*. On the other hand, if the load decreases without reach the critical load, as indicated in Figure2.9 (b), the column has an *unstable post-buckling* curve.

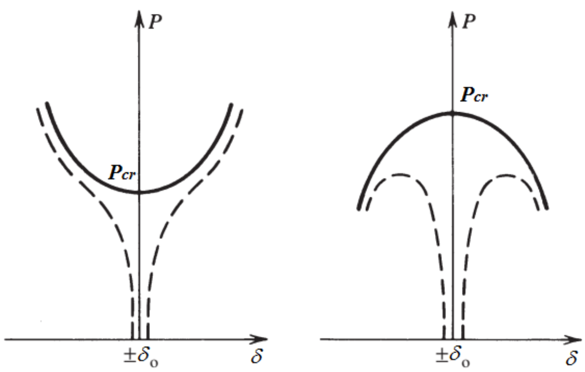

(a) (b)

Figure 2.9. Elastic post-buckling equilibrium paths of initially imperfect (dashed lines) and perfect (solid lines) systems: (a) stable and (b) unstable post-buckling (ZIEMIAN 2010).

It can be drawn that small imperfections do not significantly affect the behaviour of systems with stable post-buckling. However, it has a marked effect on systems with unstable post-buckling. These later structures are referred as *imperfection sensitive* (ZIEMIAN, 2010).

LANDESMANN & CAMOTIM (2013) reported results of numerical analysis on the influence of the cross-section geometry and end support conditions on the post-buckling behaviour of columns buckling and failing in distortional modes. The columns analyzed exhibit (i) fixed (F), pinned-fixed (P-F), pinned (P) and fixed-free (F-F) end support conditions and (ii) plain lipped channel (C), hat-section (H), zed-section (Z), and rack-section (R) cross-section shapes. Figure 2.10 plots, for F and F-F columns, the applied load (P) against the normalized displacement $|\delta|/t$, where $|\delta|$ is the maximum absolute transversal displacement occurring at the flange-lip edges and t is the wall thickness. Among other results, they concluded that the post-buckling strength decreases along the column end support condition sequence F, P-F, P and F-F. In addition, even though they expected always stiffer R columns (they have more material than their C–H–Z counterparts) this was not the case, since the extra stiffeners may have added distortional vulnerability to the column.

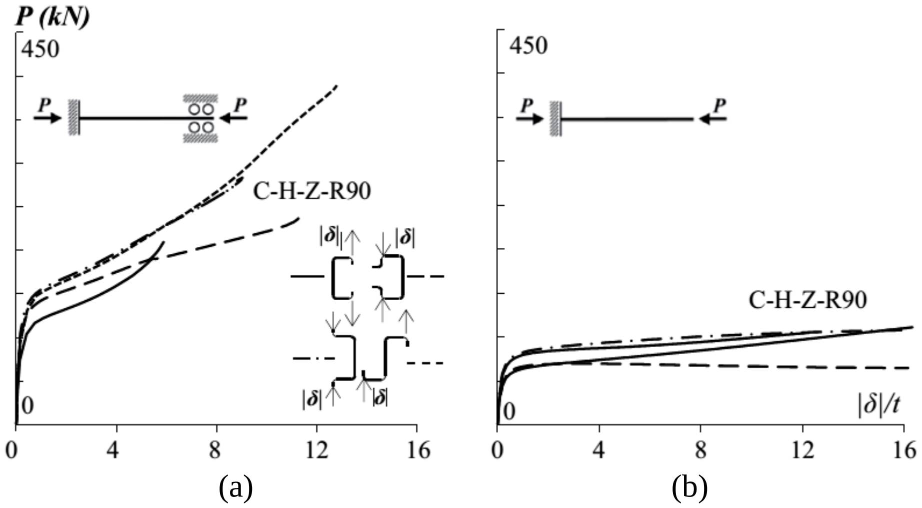

Figure 2.10. Elastic equilibrium paths P *vs.* $|\delta|/t$ concerning the C–H–Z–R90 columns with the (a) F and (b) F-F end support conditions (LANDESMANN & CAMOTIM 2013).

All these curves in Figure 2.10 represent elastic equilibrium paths. The ultimate load in which the collapse occurs is not indicated. To determine the failure load of a real member it is necessary to take initial imperfections into account, to consider the entire nonlinear load-deflection curve of the member and the material and geometrical nonlinearity. In most cases, the collapse in steel structure occurs due to an interaction between instability and plasticity phenomena. Thus, collapse occurs due to instability in elastic-plastic stage (REIS & CAMOTIM, 2001). Hence, it is necessary to assess the elastic-plastic post-buckling behaviour.

When a compression member loses the ability to support increasing load and the deflection keep increasing then the ultimate load was already reached. This load is the peak of the elastic-plastic post-buckling equilibrium path. Figure 2.11 plots the applied load normalized ($P/P_{cr.D}$) against $|\delta|/t$ as an example of elastic-plastic equilibrium path of F and P-F columns. After the peak (white circles), the column is not able to support more load. Instead, the load decreases while the deflection increases. This peak indicates the highest value of ratio $P/P_{cr.D}$, and in this case P is the ultimate load (named as P_u). As the $P_{cr\,D}$ is easily obtained from the linear buckling analysis, the evaluation of the ultimate load is straightforward.

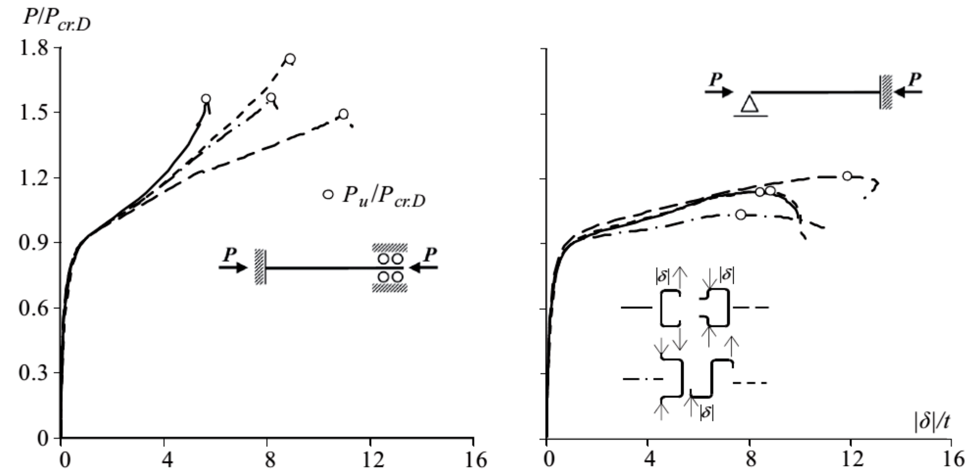

(a) (b)

Figure 2.11. Elastic-plastic distortional equilibrium paths ($P/P_{cr.D}$ *vs.* $|\delta|/t$) concerning the (a) F and (b) P-F of C–H–Z–R90 columns (LANDESMANN & CAMOTIM 2013).

It is worth to mention that the ultimate strength is related to the yield stress (f_y). When the f_y increases, the P_u increases as well, as indicated in Figure 2.12. It can also be noticed that for the same yield stress, the columns with intermediate stiffeners present higher ultimate loads.

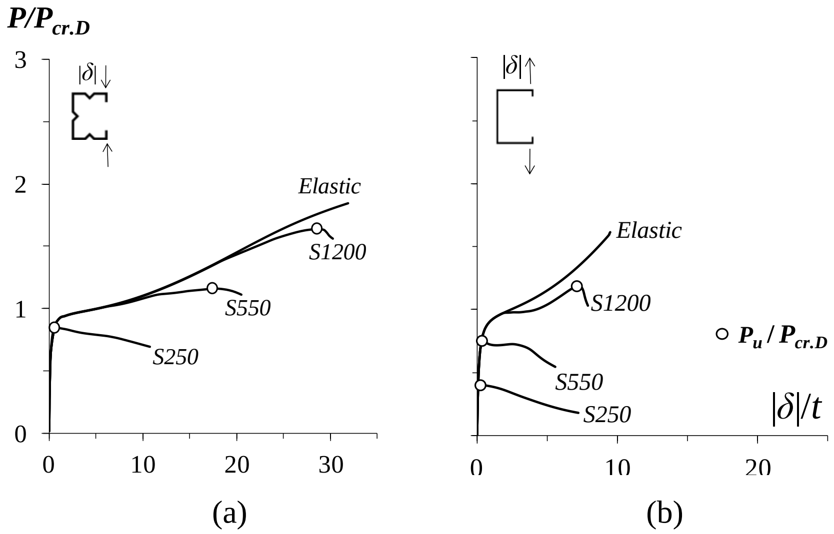

Figure 2.12. Elastic-plastic distortional equilibrium paths ($P/P_{cr.D}$ *vs*. $|\delta|/t$) concerning (a) SLC and (b) PLC with f_y*=250-550-1200MPa* (GARCIA *et al.*, 2014).

2.1.2 Distortional buckling

Distortional buckling of thin-walled members in compression is characterized by rotation of the web-flange junction in members with edge stiffeners for plain cross-section (Figure 2.13(a)), but for intermediate stiffened lipped cross-section, the intermediate stiffener moves normally to the element plan, as shown in Figure 2.13(b) (SCHAFER, 2000).

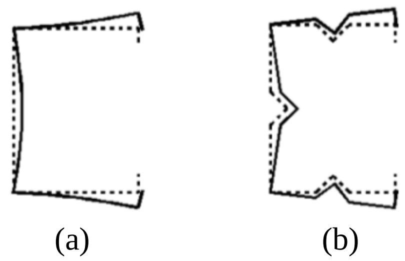

Figure 2.13. In-plane distortional mode for (a) PLC and (b) SLC column.

Although thin-walled cross-section have been studied since 1940's, at that time the distortional bucking was too complicated to be predicted analytically. It was in the 80's and 90's that studies concerning distortional buckling were intensified.

LAU & HANCOCK (1987) developed analytical expressions for distortional buckling stress of thin-walled channel columns of general cross-section geometry in order to permit explicit evaluation of buckling stresses by designers.

KWON & HANCOCK (1992) carried out compression tests on plain lipped channel and on web stiffened lipped channel columns with fixed-end boundary conditions. This work provided a design curve for members undergoing distortional buckling. The authors also observed a significant post-buckling strength reserve in the distortional mode, even when local and distortional buckling occurred simultaneously.

HANCOCK *et al.* (1994) described tests on a range of thin-walled CFS cross-sections (Figure 2.14) performed at University of Sydney to determine the strength of members failing in the pure distortional buckling mode, or the distortional-local buckling interaction. The authors proposed two sets of design curves for CFS members.

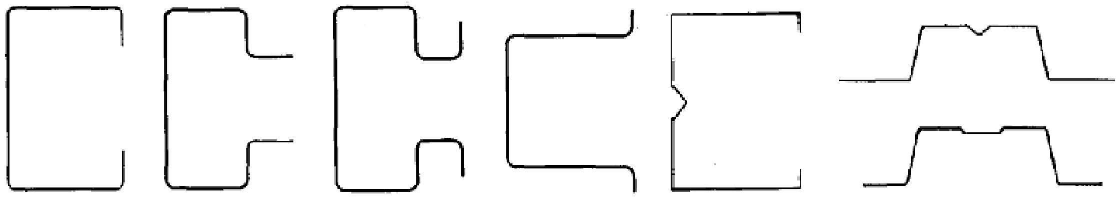

Figure 2.14. CFS cross-sections considered in tests at University of Sydney (HANCOCK *et al.*, 1994).

The distortional mode is prevalent, in a typical lipped channel column, when the flange width approximates of the web height. Then the distortional strength decreases and the local strength increases at the same time. Thus, sections approximately square tend to present higher distortional mode participation. Cross-section with narrow flanges (less than 1/6 of web height) is in general controlled by local buckling mode.

Adding longitudinal intermediate stiffeners in the cross-section elements increases considerably the local buckling strength and the distortional buckling mode become prevalent. In addition, for PLC columns, distortional mode is not prevalent in long lips cross-sections. Although a decreased in the critical distortional buckling is noticed when the lip is elongated, the critical local load presents a decrease much more remarkable. Hence, long lips retard distortional mode and trigger local mode. Also, members with distortional failure have higher imperfection sensitivity, have lower post-buckling capacity than local failures and distortional buckling may control the failure mechanism even when the elastic distortional buckling stress is higher than the local one (SCHAFER, 2000).

Aiming at evaluating the distortional buckling and post-buckling behaviour of stiffened columns and asses the design standards, YANG & HANCOCK (2004) performed a series of compression tests on web-flange stiffened lipped channel (SLC) columns fabricated with high strength steel of thickness *0.42mm* with nominal yield stress *550MPa*. A range of lengths were tested between fixed ends to determine the strength of the sections. The tests indicated that distortional buckling and the interaction of local and distortional buckling may have a significant effect on the strength of the sections formed from such thin high strength steel. These authors used the Effective Width Method and the Direct Strength Method, neither of which account for interaction of local and distortional buckling

a) Stiffened channel x plain channel

As mentioned previously, the quantity of buckling modes depends on the number of walls and intermediate nodes considered in discretization. Thus, it is possible to obtain more or less distortional buckling modes adding or eliminating elements. For example, SLC cross-section has *15* natural nodes (*14* walls) and Figure 2.15 shows the main buckling modes for column with this type of cross-section. Thus, **1** to **4** modes (GBTUL numbering) are global buckling, **5** to **15** are distortional buckling modes and the remaining deformed configurations are local buckling modes.

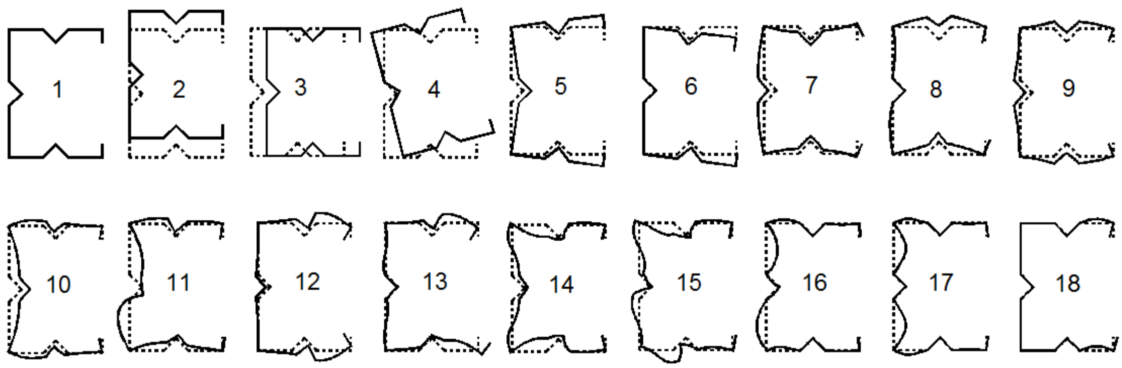

Figure 2.15. In-plane deformed configuration of web-flange stiffened lipped channel column in centered compression.

The SLC presents higher strength than its plain counterpart, this is well known and it was largely addressed in many studies (*e.g.* HOON *et al.* 1993, SCHAFER & PEKÖZ 1997, EL-SHEIKH *et al.* 2001 and HAIDARALI & NETHERCOT 2012). However, recent studies found a particular post-buckling behaviour for SLC columns under distortional mode.

Numerical analysis carried out by SILVESTRE & CAMOTIM (2006) showed that the distortional post-buckling behaviour is asymmetric in SLC columns. These authors noticed that simple supported stiffened columns present asymmetric distortional elastic post-buckling behaviour concern to it plain counterpart concerning to the flange-lip motion (Figure 2.16(a)). Although this behaviour is less relevant in fixed columns the post-buckling asymmetry is also visible in this case (Figure 2.16(b)). While local post-buckling behaviour for plain or stiffened members is quite similar, the distortional behaviour is clearly different. The PLC column exhibits a higher post-critical strength for inward displacements and SLC column for outward displacements. The same asymmetry was also noticed by (i) YANG & HANCOCK (2003, 2004, 2006) who carried out experimental and numerical studies for fixed columns with intermediate stiffeners in the web and flanges and (ii) SILVESTRE *et al.* (2005) that numerically studied simply-supported columns with several (plain and stiffened) cross-section geometries.

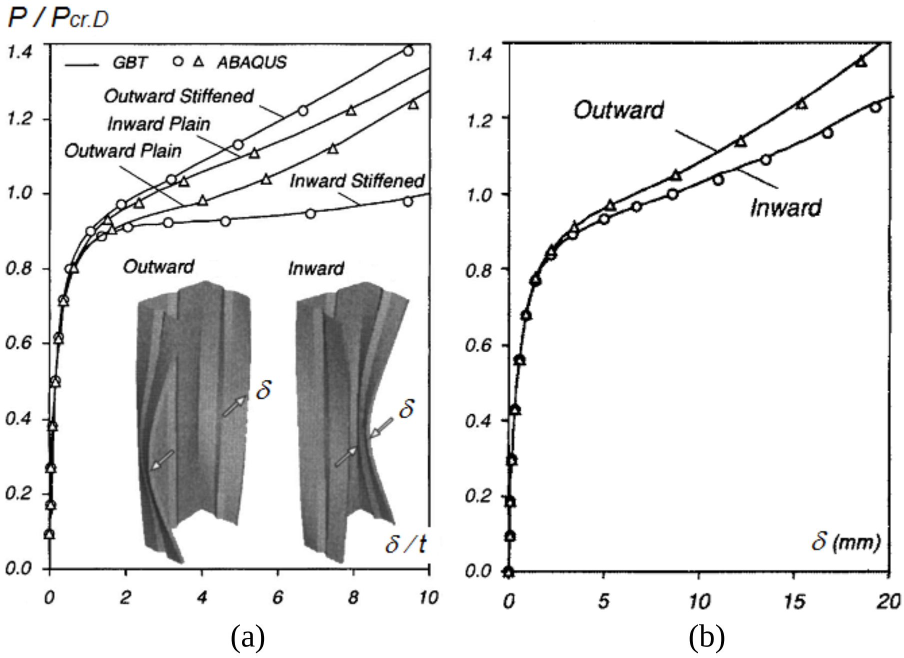

Figure 2.16. Distortional elastic post-buckling equilibrium paths for (a) pinned SLC and PLC and (b) fixed SLC columns (SILVESTRE & CAMOTIM, 2006).

2.2 Design methods

The emphasis in the next section is on design methods for ultimate strength prediction of cold-formed steel members, especially the Direct Strength Method. Three design methods are currently provided in Brazilian specification for cold-formed steel: the classical Effective Width Method, the Effective Sections Method and the recently developed Direct Strength Method.

2.2.1 Effective Width Method (EWM)

Traditionally used until 1990's for design and safety check of CFS the EWM takes each element considering that just a portion of this element contributes to the member strength. Originally it was proposed by *Von Karman* and adopted for CFS member by *Winter* at Cornell University (HANCOCK *et al.*, 2001). However, the EWM (i) ignores inter-element (*e.g.* between the flange and the web) equilibrium and compatibility in determining the elastic buckling behaviour, (ii) incorporation of competing buckling modes, such as distortional buckling can be awkward, (iii) cumbersome iterations are required to determine even basic member strength and (iv) determining the effective section becomes increasingly more complicated as attempts to optimize the section are made (when the cross-section geometry become more complex, for example adding intermediate stiffeners, the calculation of effective width is more difficult as well) (SCHAFER, 2008).

Also, the EWM is often not appropriate to account distortional buckling. In 1992 the design method in the AISI Specification was proved as unconservative for distortional buckling of channel sections composed of high-strength steel and so alternative design methods were necessary to design against distortional buckling in this case (HANCOCK *et al.*, 1994). Furthermore, SCHAFER & PEKÖZ (1997) compared existing experimental data and design specifications and concluded that existing standards were unconservative, particularly for cross-sections with multiple intermediate stiffeners.

2.2.2 Effective Section Method (ESM)

The Effective Section Method, ESM, is an extension of the Effective Area Method (EAM) which was originally proposed for cold-formed columns. Indeed, the qualities of the EAM are the same found in the direct strength method: (i) the local plate buckling is taken by considering the complete cross-section behaviour, unlike the EWM rules for isolated plate elements; (ii) there are structural resistance curves for columns, including local-global buckling interaction and (iii) rules for design were formulated as in DSM (see next section). The extension of the effective area method principles to cold-formed beams permitted the proposition of rules and equations to be applied for the design of steel cold-formed members which could replace the EWM (BATISTA, 2010).

The Effective Section Method (ESM), also included in the Brazilian Standard (ABNT, 2010), considers an effective area evaluation instead of taking each one of the cross-section elements separately. Thus, the ESM is simpler than the EWM.

2.2.3 Direct Strength Method (DSM)

Unlike the EWM, the Direct Strength Method (DSM) does not consider effective width calculations. The DSM uses gross properties of a member to evaluate the member strength but requires an accurate calculation of member elastic buckling behaviour. Numerical methods, such as GBTUL or ANSYS, easily provide the required stability calculations. In addition, the ESM provides direct equations to obtain local buckling results for usual CFS members. The reliability of the DSM equals or betters the traditional EWM for a large database of tested beams and columns (SCHAFER, 2008).

The DSM was developed in order to surpass the difficulties related to intrinsic calculations of EWM making CFS design easier and faster. SCHAFER (2002) - which summarizes the work done by SCHAFER (2000) - joined existing numerical results available in literature to his own numerical analysis concerning great variety of cross-section columns (Figure 2.17).

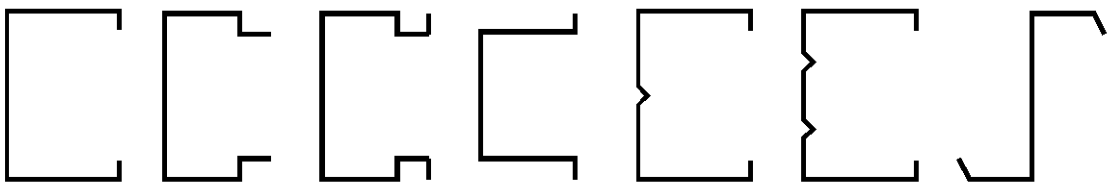

Figure 2.17. Cross-section column geometries considered by SCHAFER (2000).

Different design curves for local and distortional buckling modes were proposed (Figure 2.18). Note that for the local failures the normalization of P_{test} is to P_e, the maximum strength due to global buckling (thus reflecting local–global interaction), while for distortional buckling the normalization of P_{test} is to P_y, the squash load of the column (SCHAFER, 2008).

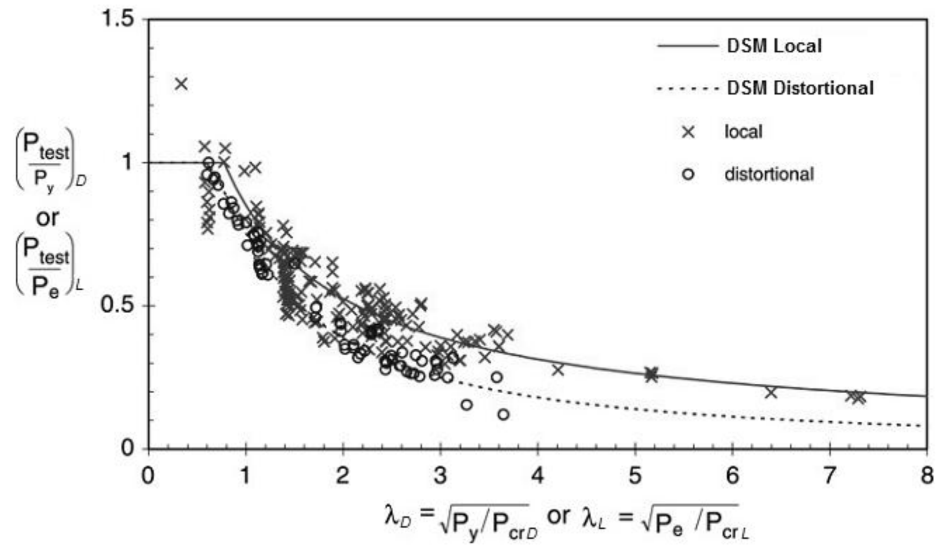

Figure 2.18. Slenderness (λ) *vs.* strength of all available column data (SCHAFER, 2008).

The DSM curve addressed to ultimate strength prediction of columns failing in distortional mode is expressed by Equations (2.4) and (2.5).

$$P_{n.D} = P_y \text{, for } \lambda_D \leq 0.561 \quad \text{(Eq. 2.4)}$$

$$\frac{P_{n.D}}{P_y} = \left(1 - 0.25\left(\frac{P_{cr.D}}{P_y}\right)^{0.6}\right)\left(\frac{P_{cr.D}}{P_y}\right)^{0.6} \text{, for } \lambda_D > 0.561 \quad \text{(Eq. 2.5)}$$

Due to its simplicity and efficiency, the DSM has been widely disseminated. Indeed, it was already incorporated to Brazilian standards (ABNT, 2010), American standards (AISI, 2012) and Australian/New Zealand (AS/NZS, 2005). According to Brazilian specification, the design of thin-walled CFS members under centered compression and distortional mode can be done using the following expressions - which are just a rearrangement of equations (2.4) and (2.5). The value of $P_{cr.D}$ is easily obtained from elastic buckling analysis, through GBTUL or ANSYS.

$$P_{n.D} = Af_y \text{, for } \lambda_D \leq 0.561 \quad \text{(Eq. 2.6)}$$

$$P_{n.D} = \left(1 - \frac{0.25}{\lambda_D^{\,1.2}}\right)\frac{Af_y}{\lambda_D^{\,1.2}} \text{ , for } \lambda_D > 0.561 \qquad \text{(Eq. 2.7)}$$

$$\lambda_D = \left(\frac{Af_y}{P_{cr.D}}\right)^{0.5} \qquad \text{(Eq. 2.8)}$$

Recent investigations identified several columns exhibiting ultimate strengths that were not adequately predicted by the current DSM design curve. Such columns exhibit (i) end support conditions other than fixed (LANDESMANN & CAMOTIM 2011, 2013), (ii) cross-sections with intermediate stiffeners (YANG & HANCOCK 2004, YAP & HANCOCK 2011 and KUMAR & KALYANARAMAN 2014) and (iii) modal interaction (YANG & HANCOCK 2004, DINIS *et al.* 2012 and SILVESTRE *et al.* 2012).

More recently, KUMAR & KALYANARAMAN (2014) reported experimental results concerning *14* fixed-ended SLC columns failing in distortional modes and exhibiting (i) web-to-flange width ratios between *0.77* and *1.06*, (ii) web-to-lip width ratios comprised between *12* and *27* (*web/lip>18* for most columns) and (iii) small-to-moderate distortional slenderness values, comprised between *1.15* and *1.81*. Moreover, these authors reported results of ABAQUS numerical (finite element) analysis also concerning SLC columns (i) to simulate the columns tests and (ii) to perform a parametric study intended to generate additional distortional ultimate strength data. This parametric study consisted of *12* fixed-ended SLC columns with (i) a constant web-to-flange and web-to-lip width ratio (*web/flange=1* and *web/lip=20*) and (ii) distortional slenderness comprised between *1.00* and *1.75*. All the columns analyzed incorporated critical-mode (distortional) initial geometrical imperfections with amplitude equal to $0.94{\cdot}t$ and involving inward flange-lip motions – no residual stress and corner strength effects were considered. With the stated objective of “precluding overall buckling”, the finite element model employed had the rigid-body in-plane translations and torsional rotations prevented along the whole column length – this was achieved by means of continuous horizontal supports located along the columns web-flange longitudinal edges. Finally, on the basis of the obtained column distortional failure load data bank (*14* experimental values and *12* numerical ones) they (i) concluded that the currently codified DSM distortional strength curve provided excessively safe failure load estimates for SLC columns and, (ii) proposed an alternative DSM design curve ($P_{n.DP}$) intended to predict distortional failures of SLC columns, according to Equations (2.9) and (2.10).

$$P_{n.DP} = P_y \text{, for } \lambda_D \leq 0.474 \qquad \text{(Eq. 2.9)}$$

$$\frac{P_{n.DP}}{P_y} = \left(1 - 0.23\left(\frac{P_{cr.D}}{P_y}\right)^{0.3}\right)\left(\frac{P_{cr.D}}{P_y}\right)^{0.3} \text{, for } \lambda_D > 0.474 \qquad \text{(Eq. 2.10)}$$

Figure 2.19 shows a set of curves (P_u/P_y *vs.* λ_D): (i) MDSM-DB - the design curve suggested by KUMAR & KALYANARAMAN (2014), (ii) DSM-DB - the current design curve, (iii) the elastic buckling curve and (iv) experimental (test) and numerical (FEA) results reported by these authors. Note that the two design curves for distortional buckling exhibit similar format and the equations that define them only differ in three coefficients.

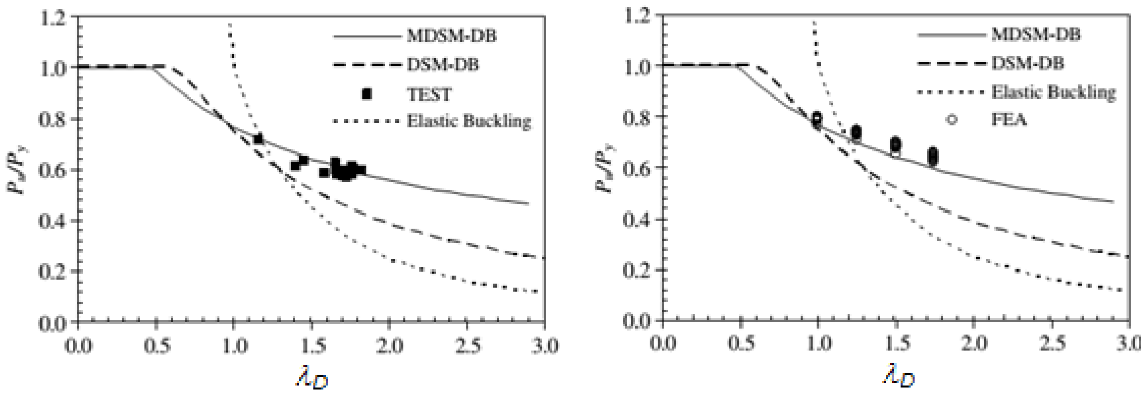

(a) (b)

Figure 2.19. DSM design curves: MDSM-DB, DSM-DB, elastic buckling curves and (a) experimental result; (b) numerical result (KUMAR & KALYANARAMAN, 2014).

It should be mentioned that the proposed design curve (i) lies well above the currently codified (AISI, 2012) DSM distortional design curve, which is supposedly applicable to predict the distortional failures of columns with any cross-section shape and (ii) lies also above the currently codified DSM local design curve[6].

[6] These authors had previously proposed a new DSM local strength curve for SLC columns (KUMAR & KALYANARAMAN, 2012). Nevertheless, these authors (KUMAR & KALYANARAMAN, 2014)

In order to enable a visualization of how "revolutionary" this strength curve is, Figure 2.20 shows a comparison between (i) the currently codified DSM local (P_u/P_y *vs.* λ_L – DSM-L) and distortional (P_u/P_y *vs.* λ_D – DSM-D) design curves, and (ii) the proposed distortional strength curve (P_u/P_y *vs.* λ_D – DSM-DP). It is observed that:

(i) Except for quite stocky columns, the DSM-DP curve always lies above its DSM-D counterpart. Moreover, the differences quickly become quite large and keep growing as λ_D increases – recall the KUMAR & KALYANARAMAN (2014) did not analyze any SLC column with λ_D higher than *1.81*.

(ii) For slenderness values higher than about *1.5*, the DSM-DP curve lies above the DSM-L one, which is really surprising, in view of the well-known fact that the column local post-critical strength reserve significantly exceeds its distortional counterpart[7].

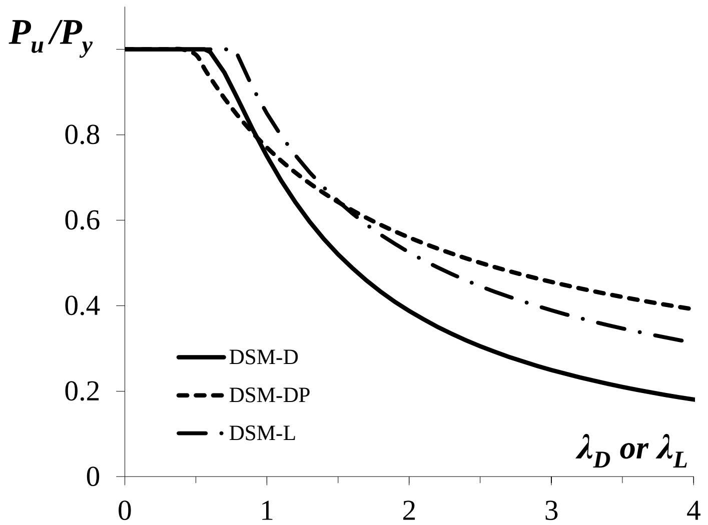

Figure 2.20. Comparison between the distortional strength curve proposed by KUMAR & KALYANARAMAN (2014) and the currently codified DSM local and distortional design curves.

After studying closely the work reported by KUMAR & KALYANARAMAN (2014), it is possible to identify some questionable issues that are bound to influence, to a smaller or larger extent, the conclusions drawn in the above paper – in particular, the

state explicitly that "*The post-distortional buckling strength (of the SLC columns) can be greater than the post-local buckling strength* of the *lipped channel (PLC) columns section, having the same value of the respective nondimensional slenderness ratios, particularly for sections having smaller values of web/flange ratio*".

[7] Apparently, KUMAR & KALYANARAMAN (2012) "solved" this discrepancy by proposing a new DSM local strength curve for SLC columns that lies above the DSM-L curve.

need to use specific DSM design curve for designing SLC columns against distortional failure. These issues are briefly summarized next:

(i) The authors performed numerical analysis of columns with the rigid-body in-plane translations and torsional rotations prevented along the whole length. However, these additional support conditions are not present in the experimental tests reported. The aim of ensuring “pure” distortional deformations up to the failure load does not seem appropriate, particularly because it unduly eliminates the minor-axis bending caused by a possible effective centroid horizontal (normal to the web) shift, which should not be artificially removed from the column distortional post-buckling behaviour. Naturally, these additional support conditions render the columns stiffer and, therefore, increases their failure loads – the experimental failure loads reported by KUMAR & KALYANARAMAN (2014) were overestimated by the corresponding numerical simulations (a few illustrative examples are presented in Section 4.2).

(ii) The columns analyzed, experimentally or numerically, cover a quite limited (small-to-moderate) distortional slenderness range, comprised between *1.00* and *1.81*.

(iii) The numerical results presented concern *12* columns, all exhibiting the same web-to-lip width ratio (*web/lip=20*). Even if the experimental failure loads correspond to columns with *web/lip* comprised between *12* and *27*, a relevant range is not adequately covered.

3 Column Selection and Buckling Behaviour

This chapter details the method and criteria adopted for column selection procedure and shows results from buckling analysis. All columns analyzed are listed, indicating the cross-section dimensions and the length adopted, some signature curves and modal participation of the most relevant buckling modes for SLC are also presented.

3.1 Column geometry selection and buckling analysis

The first stage of this work consisted of careful selecting the cross-section dimensions and lengths of the fixed-ended SLC and PLC columns to be analyzed. The selection procedure, which involved sequences of "trial-and-error" buckling analysis, was performed using mostly code GBTUL (BEBIANO *et al.* 2010a,b), but also ANSYS shell finite element models, and aimed at satisfying the following requirements:

(i) Columns buckling in "pure" distortional modes and also exhibiting distortional collapses. This goal is achieved by ensuring that the critical buckling load (i_1) is clearly distortional and (i_2) falls considerably below the lowest local and global bifurcation loads.

(ii) Cross-section dimensions involving different wall width proportions, namely web-to-flange and web-to-lip width ratios. This requirement is intended to enable the assessment of whether such width proportions have a meaningful influence on the column distortional post-critical strength and failure load.

(iii) Column lengths associated with single half-wave distortional buckling mode.

Before showing the results of this column selection procedure, it is worth presenting and discussing some SLC columns GBT-based buckling results, with the objective of clarifying the choices adopted in this work concerning the meaning of the words "local buckling" and "distortional buckling". First of all, it is commonly agreed that distortional deformations are associated with in-plane transverse displacements of cross-section internal corners (member folded line). According to this definition, which was formulated having basically plain cross-sections in mind, and taking advantage of the GBT modal language, it can be said that PLC and SLC columns buckle in a "pure" distortional mode when the corresponding buckling mode shape exhibits a dominant contribution from one or more of the deformation modes depicted in Figures 3.1(a) (PLC) or 3.1(b) (SLC), which is often combined with a more or less minor contribution from the local deformation modes shown in Figures 3.2(a) (PLC) or 3.2(b) (SLC).

The comparative analysis of the PLC and SLC (cross-section) GBT deformation modes, provided in Figures 3.1(a)-(b) and 3.2(a)-(b), draws the following remarks:

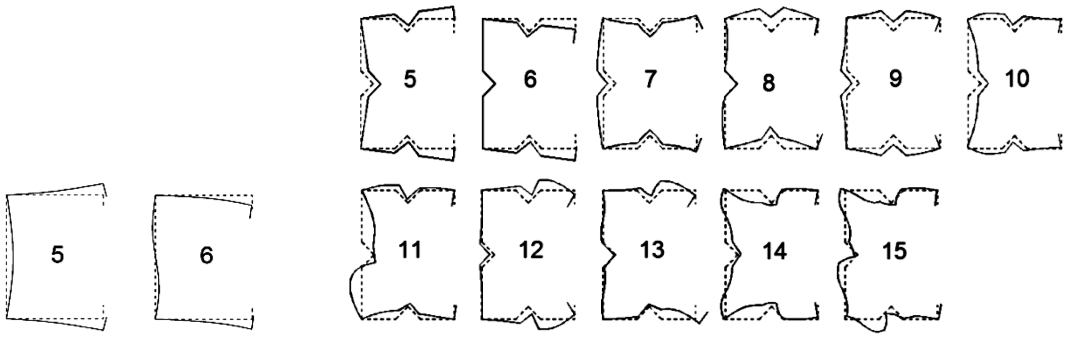

(a) (b)

Figure 3.1. GBT distortional deformation modes of (a) PLC and (b) SLC cross-section.

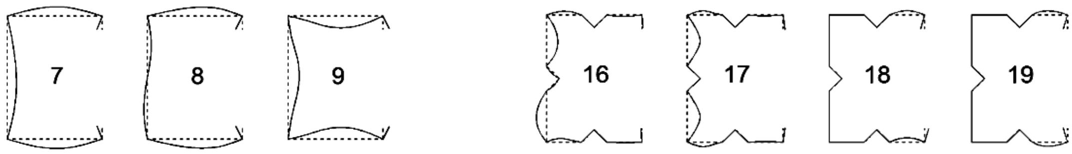

(a) (b)

Figure 3.2. Most relevant GBT local deformation modes of (a) PLC and (b) SLC cross-section.

(i) The number of distortional deformation modes is significantly higher in the stiffened columns, which is due to the additional number of internal corners stemming from the presence of the intermediate stiffeners. While in the plain columns there are only *2* distortional deformation modes (one symmetric and the other anti-symmetric), the stiffened columns exhibit the amount of *11* distortional deformation modes.

(ii) Some stiffened cross-section distortional deformation modes strongly resemble plain local deformation modes (if the presence of the stiffeners is "ignored"). The shapes of the stiffened and plain deformation modes **7**, **8** and **9** depicted in Figures

3.1(b) and 3.2(a), are clearly similar – the only difference is the presence of “partially effective” stiffeners, in the sense that they are unable to prevent the in-plane transverse displacements of the web and flange mid-points.

(iii) Although all the stiffened “distortional” deformation modes displayed in Figure 3.1(b) abide to the definition aforementioned, an adequate structural assessment must treat them separately. For instance, the DSM distortional design curve aim at predicting ultimate strengths of members exhibiting collapse modes akin to combinations of deformation modes **5** and **6** – collapse modes involving dominant contributions from deformation modes **7** to **15** should be handled by DSM local design curve.

(iv) In accordance to the content of the previous item, this work makes a distinction between the buckling behaviours involving deformations akin to modes **5** and **6** and **7** to **15**.

The end products of the “trial-and-error” procedure were the *23* SLC columns cross-section dimensions given in Table 3.1 and illustrated in Figure 3.3(a). One notices that (i) sections SLC-50-100(1)-150 and SLC-120(1)-120(2)-120(3)-140-140(1) were previously analyzed by KUMAR & KALYANARAMAN (2014), by means of numerical[8] and experimental approaches, respectively, (ii) the web-to-flange width ratio (h/b) ranges from *0.85* to *1.33*, (iii) the web-to-thickness ratio (h/t) ranges from *37.5* to *95.6*, (iv) the web-to-lip ratio (h/d) ranges from *6.67* to *26.84*, (v) the web intermediate stiffener width-to-depth ratio (s_{1w}/s_{2w}) varies from *2.0* to *2.6*, (vi) the flange intermediate stiffener width-to-depth ratio (s_{1f}/s_{2f}) varies from *2.0* to *2.58*, (vii) the web-to-stiffener width ratio (h/s_{1w}) varies from *3.7* to *8.0*, and (viii) the flange-to-stiffener width ratio (b/s_{1f}) varies from *3.9* to *8.0*.

Moreover, *20* PLC columns, given in Table 3.2 and illustrated in Figure 3.3(b), included in this work for comparison proposes (i) were previously numerically analyzed by LANDESMANN & CAMOTIM (2013) or SANTOS *et al.* (2014), (ii) the web-to-flange width ratio (h/b) ranges from *0.7* to *1.83*, (iii) the web-to-thickness ratio (h/t) ranges from *30.0* to *75.47*, (iv) the web-to-lip ratio (h/d) ranges from *6.0* to *18.87*.

[8] Indeed, the SLC-50-100(1)-150 columns’ lengths were modified in order to obtain single half-wave distortional buckling modes – *i.e.*, shorter members were adopted in the present work.

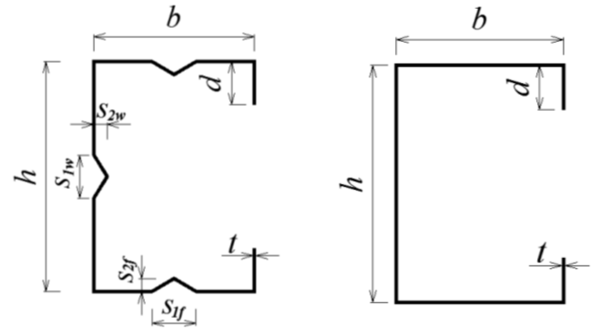

(a) (b)

Figure 3.3. Cross-section of (a) SLC and (b) PLC columns.

Table 3.2 provides, for PLC columns, (i) the cross-section dimensions, (ii) the length associated with critical distortional buckling (L_D), (ii) corresponding critical (distortional) buckling load ($P_{cr.D}$) and (iii) its ratios with respect to the lowest local ($P_{b1.L}$) and global ($P_{b1.G}$) bifurcation loads.

Table 3.3 provides, for the SLC columns with length L_D, (i) the critical (distortional) buckling loads obtained by means of GBTUL buckling analysis including all deformation modes, and (ii) the ratios between the lowest local ($P_{b1.L}$) and global ($P_{b1.G}$) bifurcation loads, where the values of $P_{b1.L}$ and $P_{b1.G}$ are obtained by means of GBTUL buckling analysis including only local and global deformation modes, respectively. Note that $P_{b1.L7}/P_{cr.D}$ ratio is also given, where $P_{b1.L7}$ are bifurcation loads obtained by means of GBTUL buckling analysis including deformation modes of order higher than **6** (*i.e.*, excluding only the global and "truly distortional" modes).

The buckling modes are not "purely distortional", as they exhibit more or less small contributions from deformation modes of order higher than **6** – mainly modes **7** and **9**, which are either local (PLC columns) or "treated as local" (SLC columns).

Table 3.1. Cross-section dimensions, area and Elasticity's modulus of SLC columns.

SLC	*h* (mm)	*b* (mm)	*d* (mm)	*t* (mm)	s_{1w} (mm)	s_{2w} (mm)	s_{1f} (mm)	s_{2f} (mm)	*A* (cm^2)	*E* (GPa)
50	50	50	2.5	0.579	10	5	10	5	0.97	202
50(1)	50	50	4	0.579	10	5	10	5	0.99	202
50(2)	50	50	5.6	0.579	10	5	10	5	1.00	202
65	65	65	5	0.9	10	5	10	5	1.96	210
65(1)	65	65	7.5	0.9	10	5	10	5	2.00	210
65(2)	65	65	8.5	0.9	10	5	10	5	2.02	210
65(3)	65	65	4.33	0.9	10	5	10	5	1.95	210
75	75	75	7	1.2	12	6	12	6	3.05	210
75(1)	75	65	5	2	14	7	14	7	4.65	210
80	80	80	12	2	10	5	10	5	5.53	210
90	90	90	12	1.8	18	9	18	9	5.69	210
90(1)	90	90	7	1.8	18	9	18	9	5.51	210
90(2)	90	90	4.5	1.8	18	9	18	9	5.42	210
90(3)	90	90	9.5	1.8	18	9	18	9	5.60	210
100	100	100	5	1.2	15	7.5	15	7.5	3.94	200
100(1)	100	100	5	2.145	20	10	20	10	7.18	202
120	120	90	15	1.5	20	10	20	10	5.32	200
150	150	150	7.5	2.3	30	15	30	15	11.55	202
120(1)	1220	117.19	118.6	8.62	31.96	10.91	30.94	10.91	5.65	202
120(2)	1218	116.5	129.48	5.9	31.96	10.41	31.44	10.41	5.85	202
120(3)	1219	117.87	138.55	5.82	31.96	10.91	31.45	10.91	6.15	202
140	1218	136.29	128.56	8.72	31.44	10.41	31.96	10.91	6.20	202
140(1)	1220	137.7	138.37	4.41	31.96	10.91	30.94	10.41	6.37	202

Note: all the buckling/bifurcation loads were obtained with $v=0.3$ (Poisson’s ratio)

Table 3.2. Cross-section dimensions, area, Elasticity's modulus length, critical load and local/global buckling load ratios of PLC columns.

PLC	h (mm)	b (mm)	d (mm)	t (mm)	A (cm²)	E (GPa)	L_D (cm)	$P_{cr.D}$ (kN)	$\frac{P_{b1.L}}{P_{cr.D}}$	$\frac{P_{b1.G}}{P_{cr.D}}$
60	60	60	10	2	4	210	45	247	1.49	6.17
75	75	75	10	2	4.9	210	45	212	1.37	12.87
85	85	121.4	10.6	2.65	8.97	205	50	217.5	1.54	24.94
85(1)	85	85	10.6	2.65	7.04	205	40	324.8	1.51	20.63
100	100	100	10.6	2.65	8.23	205	45	272.6	1.52	31.13
100(1)	100	142.9	10.6	2.65	10.5	205	55	184.1	1.68	39.17
100(2)	100	70	10.6	2.65	6.64	205	40	366.5	1.45	21.7
110	110	60	10	3	7.5	210	100	420	1.44	3.54
130	130	130	10.6	2.65	10.62	205	55	202.5	1.56	60.56
130(1)	130	185.7	10.6	2.65	13.57	205	70	131.6	1.77	73.49
130(2)	130	91	10.6	2.65	8.55	205	45	288	1.59	46.4
150	150	105	10.6	2.65	9.82	205	50	246.8	1.35	66.31
150(1)	150	150	10.6	2.65	12.21	205	60	174.8	1.57	90.02
150(2)	150	214.3	10.6	2.65	15.61	205	75	114.8	1.82	112.29
180	180	126	10.6	2.65	11.73	205	55	207.3	1.38	110.67
180(1)	180	180	10.6	2.65	14.59	205	70	140	1.62	141.91
180(2)	180	257.1	10.6	2.65	18.68	205	85	93.8	1.9	184.19
200	200	140	10.6	2.65	13	205	60	183.6	1.4	142.64
200(1)	200	200	10.6	2.65	18.18	205	75	124.9	1.8	189.44
200(2)	200	285.7	10.6	2.65	20.72	205	95	80.8	1.95	234.5

Table 3.3. Length, critical (distortional) load and local/global buckling load ratios and, GBT modal decomposition of SLC columns critical buckling modes.

SLC	L_D (cm)	$P_{cr.D}$ (kN)	$\frac{P_{b1.L7}}{P_{cr.D}}$	$\frac{P_{b1.L}}{P_{cr.D}}$	$\frac{P_{b1.G}}{P_{cr.D}}$	$\mathbf{p_5}$ *(%)*	$\mathbf{p_7}$ *(%)*	$\mathbf{p_9}$ *(%)*	$\mathbf{p_{others}}$ *(%)*
50	45	10.9	2.93	7.65	17.3	77.08	12.86	7.63	2.43
50(1)	45	13.1	5.44	6.45	15.1	91.33	7.05	0.18	1.44
50(2)	45	17.3	4.46	4.96	12.22	96.60	0.22	1.38	1.80
65	60	26.1	5.32	8.78	15.1	97.15	0.90	0.86	1.09
65(1)	60	36.3	3.66	6.44	11.77	95.49	2.11	1.16	1.24
65(2)	60	42.0	3.07	5.63	10.54	94.52	2.80	1.23	1.45
65(3)	50	24.7	5.52	8.95	22.52	95.07	3.28	0.40	1.25
75	60	56.2	4.74	8.34	14.8	97.22	0.59	1.10	1.09
75(1)	40	195.1	4.18	11.73	13.7	88.15	9.65	0.67	1.53
80	50	273.9	2.02	7.65	10.2	92.53	4.35	1.49	1.63
90	50	291.8	3.11	4.97	11.6	90.13	4.09	3.10	2.68
90(1)	50	164.0	4.87	8.61	18.4	86.96	11.28	0.27	1.49
90(2)	70	117.2	3.02	12.11	12.6	78.82	12.60	6.74	1.84
90(3)	70	158.6	5.12	9.18	10.26	97.27	0.55	1.19	0.99
100	80	35.3	4.62	9.00	27.7	89.54	8.32	1.13	1.01
100(1)	70	164.8	3.06	12.69	14.1	79.53	12.29	6.39	1.79
120	100	143.42	2.80	3.85	8.95	94.90	2.21	1.42	1.47
150	120	178.2	2.97	9.54	16	78.36	12.58	7.37	1.69
120(1)	122	73.1	5.55	9.83	11.7	91.52	7.64	0.07	0.77
120(2)	121.8	56.1	3.37	10.51	15.5	80.30	14.78	3.32	1.60
120(3)	121.9	53.2	3.23	9.41	17.53	79.44	15.73	3.03	1.80
140	121.8	67.5	5.12	7.73	18.6	91.77	7.16	0.22	0.85
140(1)	122	49.3	2.38	9.82	26.4	72.50	12.10	12.93	2.47

The results presented in Table 3.3 show that, as intended, all the columns analyzed in this work (i) buckle in critical distortional modes and (ii) have their first "non-distortional" bifurcation loads well above $P_{cr.D}$. Such bifurcation loads are always "local", in the sense that they correspond to buckling modes exhibiting only contributions from deformations modes of order higher than **6** (the first global bifurcation loads are always much higher). Quantitatively speaking, the values of the ratios $P_{b1.L7}/P_{cr.D}$ (SLC columns) and $P_{b1.L}/P_{cr.D}$ (PLC columns) are inside the intervals

2.02-5.55 and 1.21-1.95, respectively. In the SLC columns, the ratio $P_{b1.L}/P_{b1.L7}$ varies between 1.11 and 4.15 and the ratio $P_{b1.L}/P_{cr.D}$ varies between 3.85 and 12.69. The first global (flexural-torsional or flexural) bifurcation load is invariably quite higher (often much higher) – indeed, the $P_{b1.G}/P_{cr.D}$ values range from 8.95 to 27.7.

Figure 3.4 illustrates one of the end products obtained after performing the buckling analysis: the curves P_{cr} *vs.* L, or signature curve, (L in logarithmic scale) concerning columns with the SLC75(1) and PLC75 cross-section dimensions. The selected length value (L_D) is indicated in each figure, which also includes the corresponding distortional critical buckling mode shape. Rigorously speaking, the fixed supported column curve concerns single half-wave bifurcation loads (and not critical buckling loads). However, the critical buckling loads are associated with single half-wave buckling modes up to the length selected. Note that both columns exhibit similar single half-wave buckling mode shape.

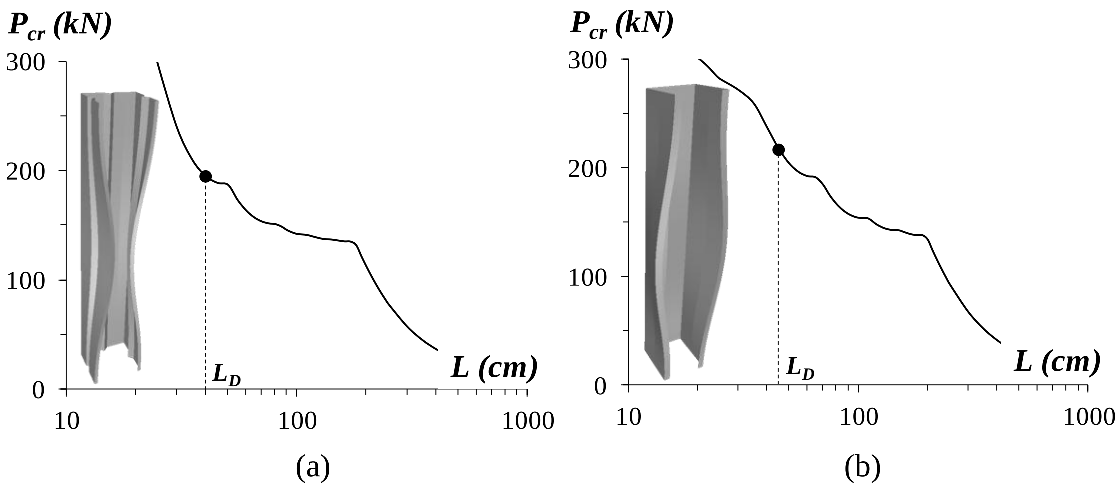

Figure 3.4. Curves P_{cr} *vs.* L concerning SLC75(1) and PLC75 columns, indicating the selected lengths (L_D) and showing the corresponding distortional buckling mode shapes.

Figure 3.5 displays the in-plane configurations of the SLC75(1) and PLC110 columns GBT deformation modes that are most relevant for the present investigation – all the remaining columns exhibit qualitatively similar deformation modes. Table 3.3 also provides the contributions of the GBT deformation modes to the critical buckling modes of all the SLC columns considered in this study – $\mathbf{p_n}$ stands for the percentage participation of GBT deformation mode **n** (this modal decomposition is illustrated in Figure 3.6, showing the buckled mid-span cross-section of the SLC90, SLC100(1) and

PLC60 columns). From the observation of these results, the following conclusions can be drawn about SLC columns:

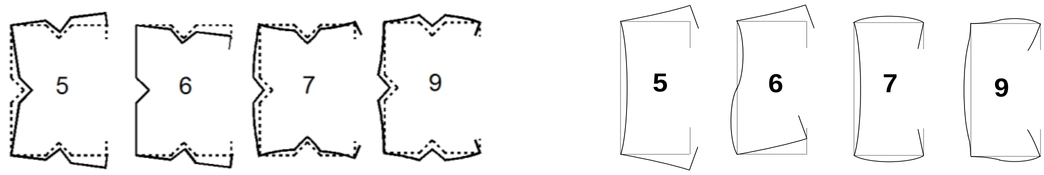

(a) SLC75(1) (b) PLC110

Figure 3.5. In-plane configurations of the SLC75(1) and PLC110 column GBT deformation modes.

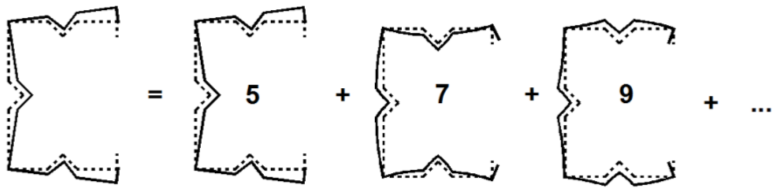

SLC90	*90.13%*	*4.09%*	*3.10%*	*2.68%*
SLC100(1)	*79.53%*	*12.29%*	*6.39%*	*1.79%*

(a)

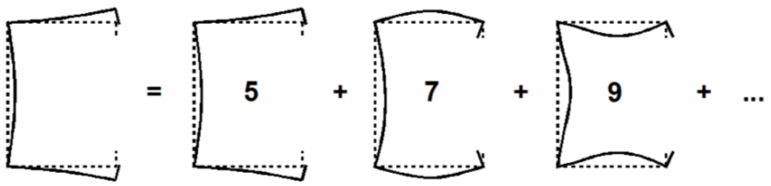

PLC60	*91.00%*	*6.93%*	*1.55%*	*0.51%*

(b)

Figure 3.6. GBT modal decomposition: distortionally buckled mid-span cross-section of the (a) SLC90, SLC100(1) and (b) PLC60 columns.

(i) All critical buckling modes combine a highly dominant participation from symmetric distortion ($\boldsymbol{p_5}$) with minor (but non negligible) contributions from local deformations ($\boldsymbol{p_7}$ and $\boldsymbol{p_9}$). While the former varies in the ranges of *72.50%-97.27%* (SLC) the joint contribution of the latter ($\boldsymbol{p_7} + \boldsymbol{p_9}$) amounts to *1.60%-25.3%*. One notices that the SLC-50-100(1)-150-120(1)-120(2)-120(3)-140-140(1) columns (these ones were considered in the work of KUMAR & KALYANARAMAN, 2014) exhibit higher participation of local mode ($\boldsymbol{p_7} + \boldsymbol{p_9}$), in the ranges of *7.38%-25.03%*. Most of them exhibit local mode participation higher than *18.10%*.

(ii) The participation of the other deformation modes never exceeds *2.68%* and is below *1.68%* in most cases.

Following the studies carried out by LANDESMANN *et al.* (2013), a correlation between the modal participation and the width ratios of the elements were assessed. Figure 3.7 shows a set of graphics relating the participation of most relevant modes (**5**, **7** and **9**) with some width ratios. The observation of these results prompts the following remarks:

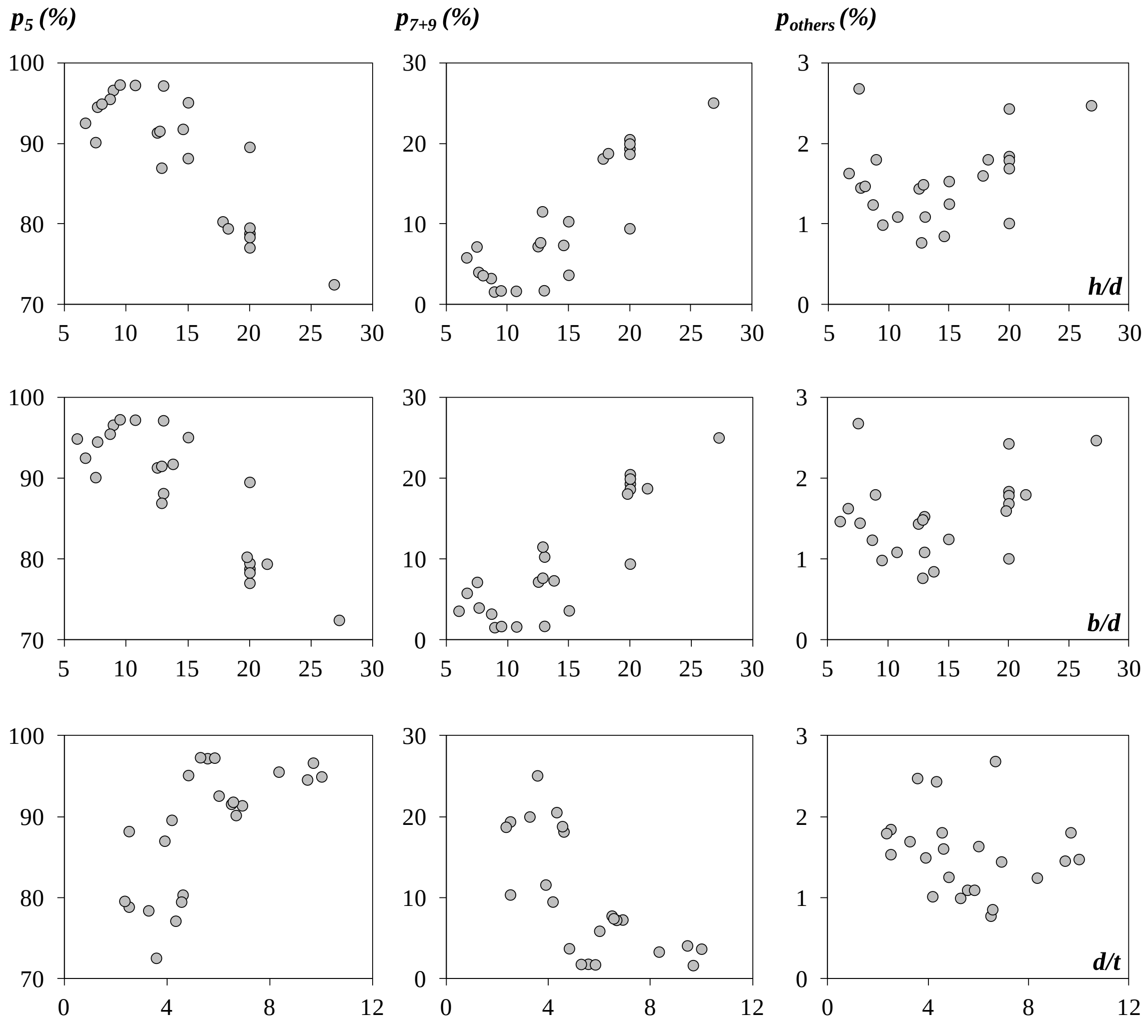

Figure 3.7. Variation of $\boldsymbol{p_5}$, $\boldsymbol{p_{7+9}}$ and $\boldsymbol{p_{others}}$ with *h/d*, *b/d* and *d/t* ratios.

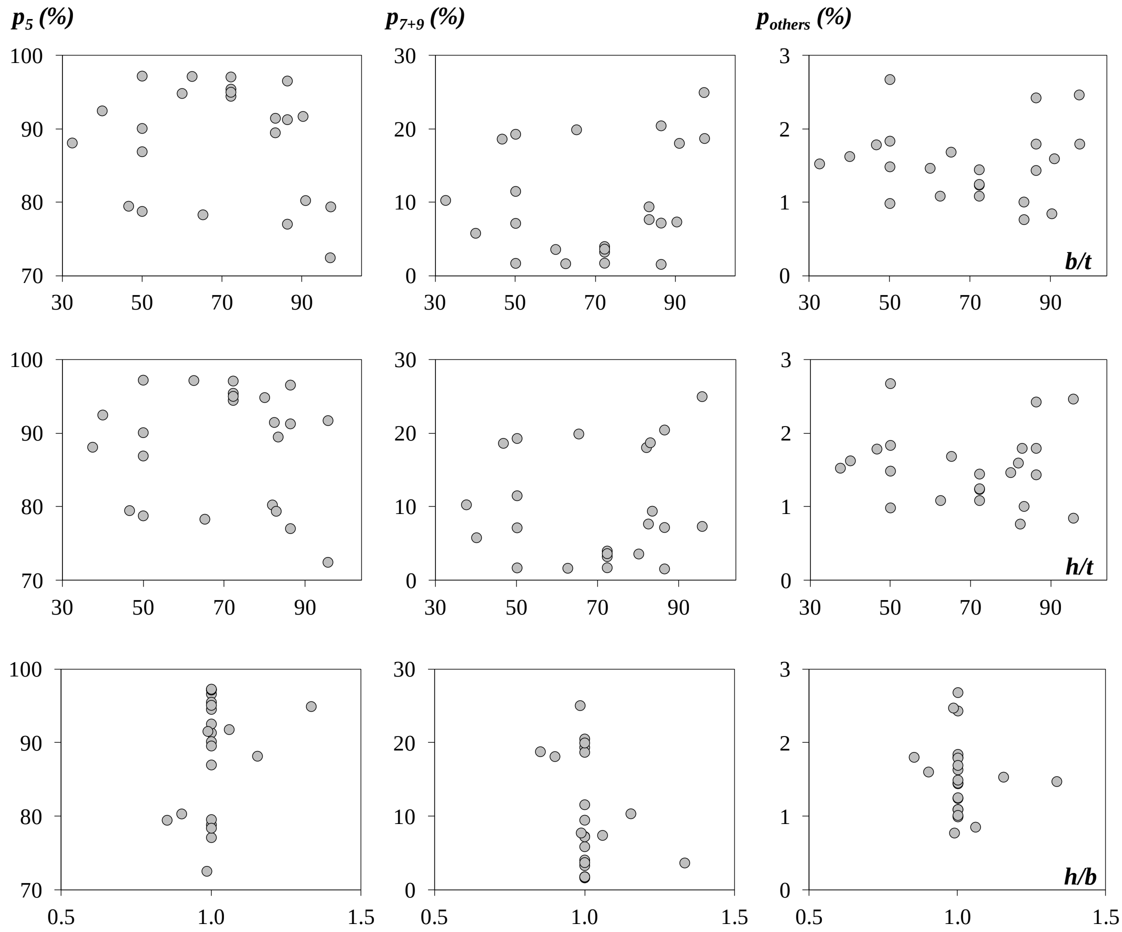

Figure 3.8. Variation of $\boldsymbol{p_5}$, $\boldsymbol{p_{7+9}}$ and $\boldsymbol{p_{other}}$ with *b/t, h/t* and *h/b* ratios.

(i) A trend of increasing in mode **5** is clear noticed when the lip dimension (*d*) is also increased (leading to lower *h/d* ratios), at the same time that joined participation of modes **7** and **9** ($\boldsymbol{p_{7+9}}$) decreases. At this point is important to mention that SCHAFER (2000) states that long lips (lower *h/d* ratio) trigger local buckling in PLC columns. However, this assertion is not valid for the SLC columns selected in this work (considering that modes **7** and **9** is treated as local buckling).

(ii) Width ratios that does not take the lip size into account are not related to any modal participation increasing or decreasing (see Figure 3.8). In fact, it may exist some correlation between the ratio *h/b* and the modal participation. However, there are no enough data to verify this assertion.

(iii) Other buckling modes ($\boldsymbol{p_{other}}$ - order higher than **9**) are irrelevant for the columns behaviour.

4 Numerical Model and Validation

After addressing the numerical (shell finite element) model adopted to perform linear and geometrically and materially non-linear analysis in item 4.1, the validation stage and discussions about the studies reported by KUMAR & KALYANARAMAN (2014) are presented in item 4.2

4.1 Finite Element Analysis (FEA)

The column distortional post-buckling equilibrium paths and ultimate strength values were determined through geometrically and materially non-linear FEA carried out in the code ANSYS (2009). The columns were discretized into *SHELL181* elements (ANSYS nomenclature – 4-node shear deformable thin-shell elements with six degrees of freedom per node and full integration) – convergence studies showed that $5mm \times 5mm$ meshes provide accurate results (Figure 4.1(a)), while involving a reasonable computational effort (GARCIA *et al.*, 2014). The analysis was performed by means of an incremental-iterative technique that combines *Newton-Raphson's* method with an arc-length control strategy (arc-length varying between 50 t and 100 t). All columns exhibited (i) critical-mode (distortional) initial imperfections with small amplitudes (*10%* of the wall thickness t) and (ii) a material behaviour either perfectly elastic or elastic-perfectly plastic (*Prandtl-Reuss* model: *von Mises* yield criterion and associated flow rule), characterized by E=200-202-210GPa (see Table 3.1), $\nu=0.3$ and several yield stresses f_y (see Table A1 to A4 – Appendix A). The vast majority of the yield stresses considered in this work are unrealistically high, leading to E/f_y that largely exceed the current DSM limit for pre-qualified columns ($E/f_y=340$). The reason for selecting such high yield stresses was to make it possible to analyze columns with high slenderness values, thus covering a wide slenderness range. No strain-hardening, residual stresses and rounded corner effects were included in the analysis.

Concerning the modeling of the end support conditions, it is worth noting that, the column end cross-section was attached to a rigid plate, thus precluding the occurrence of local and global displacements and rotations, as well as warping, as indicated in Figure 4.1(b). The axes X, Y and Z are related to the flange width, the web height and the column length, respectively.

To enable the load application, the rigid-body axial translation is free at both end sections. The axial compression (*P*) is applied by means of a concentrated force applied on the rigid plate point corresponding to fixed end sections centroid. (Figure 4.1(b)). The above forces are always increased in small increments, by means of the ANSYS automatic load stepping procedure.

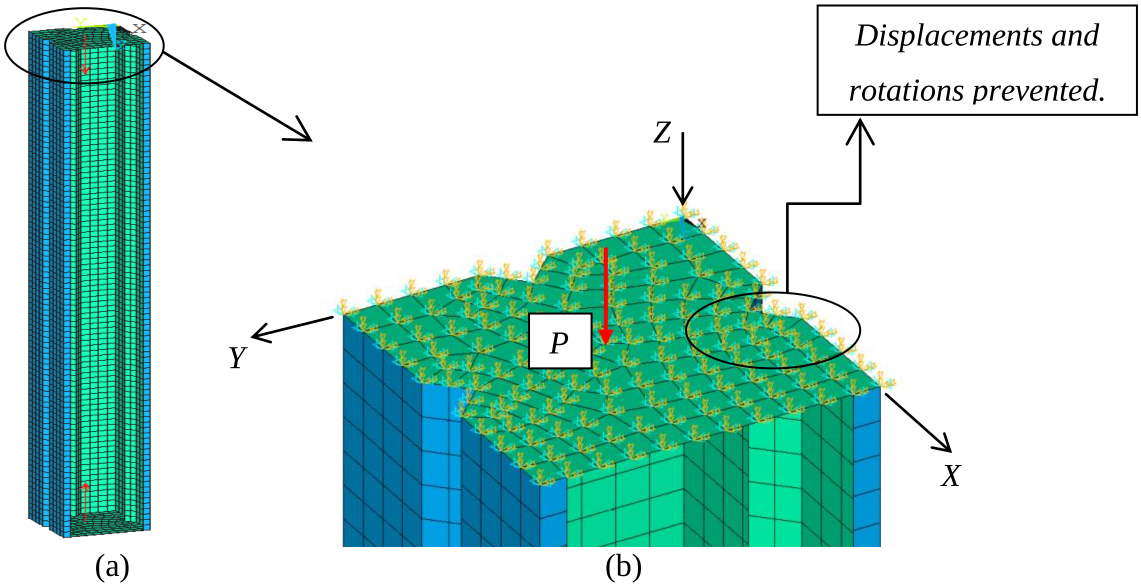

Figure 4.1. ANSYS column's model: (a) typical mesh and (b) end support conditions and applied load detail.

The incorporation of the critical-mode initial geometrical imperfections in the columns was made automatically by means of the following procedure (*e.g.*, LANDESMANN & CAMOTIM, 2013): (i) determination of the critical buckling mode shape (through ANSYS buckling analysis that adopted exactly the same discretization/mesh employed to carry out the subsequent post-buckling analysis), which was then (ii) scaled to exhibit maximum transversal displacements along the flange-lip longitudinal edges equal to $0.1\ t$ and (iii) using this buckling analysis output as input of the post-buckling (non-linear) one. The elastic post-buckling analysis was used to evaluate the flange-lip motion (inward or outward) that lead to the lower post-buckling strength condition.

The ANSYS shell finite element model validated previously by LANDESMANN & CAMOTIM (2013) and also in this work (see next section) was used to perform a parametric study aimed at assessing the elastic-plastic post-buckling behaviour and ultimate strength of SLC columns buckling and failing in distortional modes. Using the numerical results it was verified whether the current DSM curve and the curve suggested by KUMAR & KALYANARAMAN (2014) are in line with the results obtained in this work.

4.2 Validation studies

In order to use the ANSYS shell finite element model just described to assess the distortional post-buckling behaviour and strength of cold-formed steel columns, a validation step was carried out reproducing available (numerical and experimental) results reported by KUMAR & KALYANARAMAN (2014). These authors performed a total of *14* fixed-ended SLC compression tests with members that buckled and collapsed in distortional modes. In addition, *12* columns were only numerically analyzed with a set of *4* different slenderness chosen due to thickness variation. Figure 4.2(a)-(b) provide an overall view of the experimental test set-up and typical finite-element mesh used by authors in the analysis. All tested columns were manufactured in galvanized nominal grade 275 steel sheets with *1.44* mm of thickness (see Table 4.2 for the exact f_y considered in the model). The *Young's* modulus of the material was 202 *GPa* and residual stresses were not measured.

Concerning the numerical modeling adopted by KUMAR & KALYANARAMAN (2014): (i) the software used was ABAQUS, (ii) the columns were discretized by means of S4R shell finite elements (ABAQUS nomenclature – 4-node isoparametric thin-shell elements with six degrees of freedom per node and reduced shear integration), (iii) the columns were analyzed with critical-mode (distortional) initial geometrical imperfections with amplitude equal to $0.94 \cdot t$ involving inward flange-lip motions, (iv) residual stresses and corner strength enhancement effects were neglected, (v) fictitious three-dimensional B33 column elements (ABAQUS nomenclature) were used along the edges of the shell element at the two ends of the member, (vi) the overall buckling was constrained by restraining the in-plane translations and rigid body rotations at all the web-flange junction nodes along the length – as shown in Figure 4.2(b), (vii) the axial load and the end boundary conditions were imposed at the geometric centroid at the two end sections and, (viii) average properties for yield stress was determined by the *0.2%* offset method, taken from tensile coupon tests. The cross-section geometry was modeled considering mid-thickness of the plate elements - dimensions are indicated in Table 4.1 which L is the length of member.

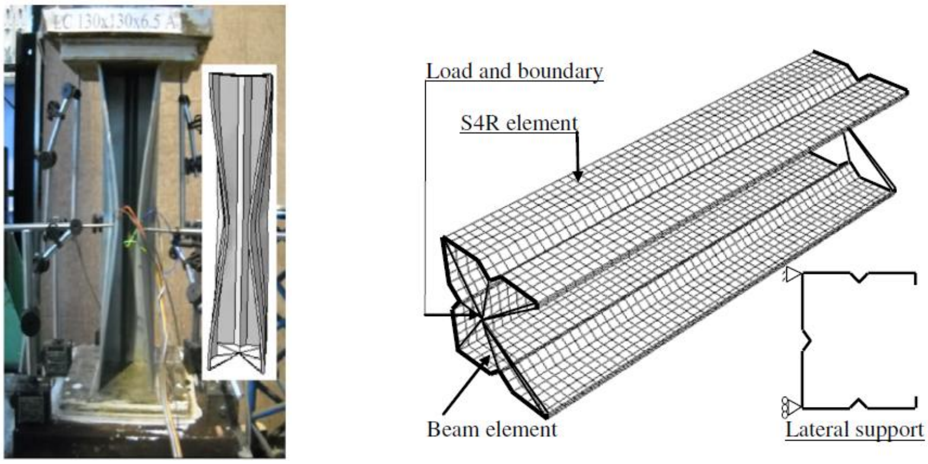

(a) (b)

Figure 4.2. (a) experimental test set up and (b) finite element used by KUMAR & KALYANARAMAN (2014).

Table 4.1. Dimensions of SLC columns analyzed in validation.

SLC	L	h	b	d	s_{1w}	s_{2w}	s_{1f}	s_{2f}
120(1)	1220	117.19	118.6	8.62	31.96	10.91	30.94	10.91
120(2)	1218	116.5	129.48	5.9	31.96	10.41	31.44	10.41
120(3)	1219	117.87	138.55	5.82	31.96	10.91	31.45	10.91
140	1218	136.29	128.56	8.72	31.44	10.41	31.96	10.91
140(1)	1220	137.7	138.37	4.41	31.96	10.91	30.94	10.41

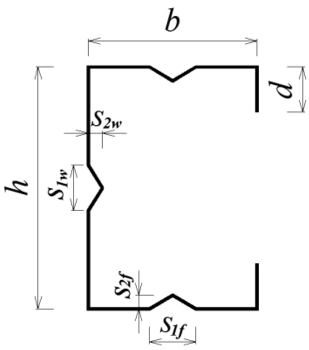

Note: Units in millimeters.

On the other hand, the numerical analysis carried out in this work for validation purposes were performed in the code ANSYS and adopted the models described in Section 4.1 – with exception of the critical-mode (distortional) initial geometrical imperfections with amplitude equal to *94%* of the wall thickness (similar to KUMAR & KALYANARAMAN model). The columns SLC-120(1)-120(2)-120(3)-140-140(1), previously presented in Tables 3.1 and 3.3, were selected for validation. For comparison purposes, these columns were also analyzed with constrained web-flange junction nodes along the length.

Figures 4.3(a)-(b) compare, for the columns SLC 120(3)-140(1) respectively, the experimental and numerical equilibrium paths relating the applied load (P) to the (i) transverse (normal to the flange) displacements (δ) of the flange-lip corner of the cross-section located *200mm* away from the column mid-height (bottom half)[9] and (ii) the column axial shortening (δ_a). Each plot displays three equilibrium paths, corresponding to (i) the experimental ($P_{KK.exp}$) and numerical ($P_{KK.num}$) results reported by KUMAR & KALYANARAMAN (2014), and (ii) the numerical results obtained in this work ($P_{TW.num}$). Note that all numerical results concern columns with the yield stresses given in Table 4.2. Moreover, the numerical results of KUMAR & KALYANARAMAN concern laterally restrained columns (see Figure 4.2(b)), unlike the experimental ones and those obtained in this work.

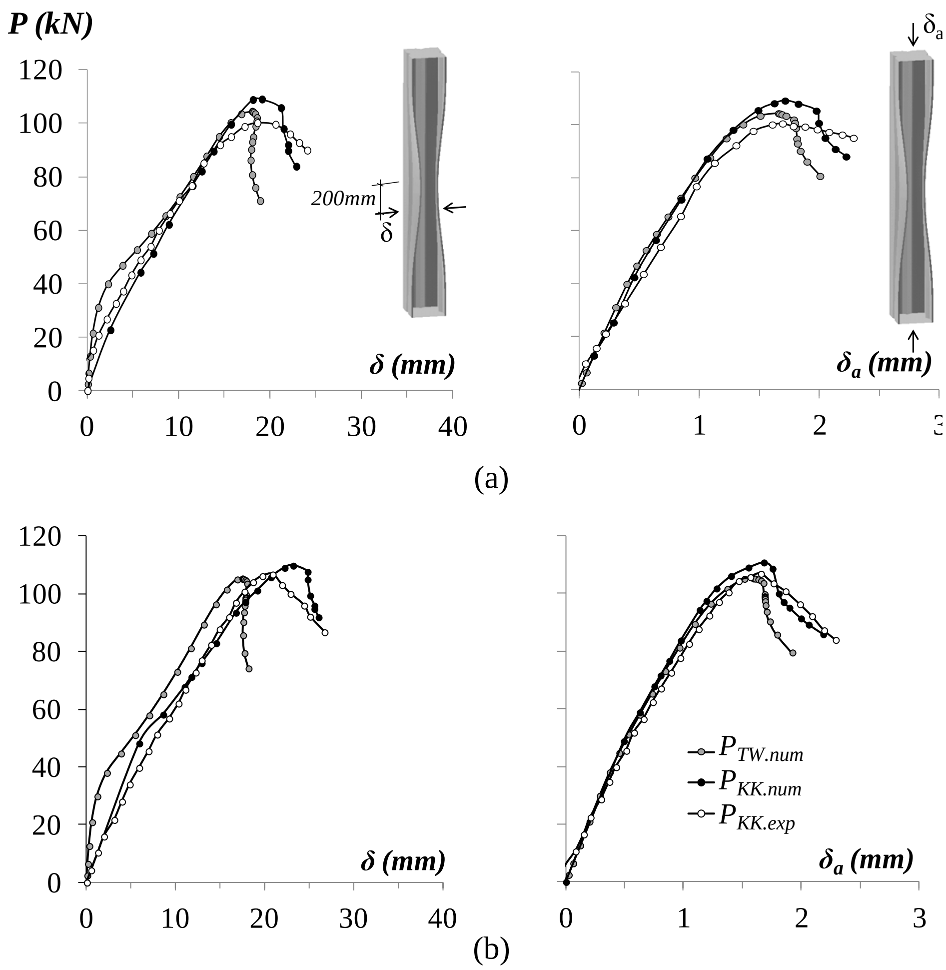

Figure 4.3. Experimental and numerical (a) SLC120(3) and (b) SLC140(1) column P *vs.* δ and P *vs.* δ_a equilibrium paths.

[9] Location of the experimental/numerical transverse displacements reported by KUMAR & KALYANARAMAN (2014).

Table 4.2 provides, for the columns SLC-120(1)-120(2)-120(3)-140-140(1), the (i) experimental and numerical failure load values reported by KUMAR & KALYANARAMAN (2014) ($P_{u.KK.exp}$ and $P_{u.KK.num}$) and (ii) numerical results obtained in this work for laterally restrained ($P_{u.TW.num.R}$) and free ($P_{u.TW.num.F}$) columns. Also, the columns yield stresses and values of the $P_{u.TW.num.F}/P_{u.KK.exp}$, $P_{u.TW.num.R}/P_{u.KK.num}$ and $P_{u.KK.num}/P_{u.KK.exp}$ ratios are shown.

Table 4.2. Failure loads reported by KUMAR & KALYANARAMAN (2014) and obtained in this work.

SLC	fy (MPa)	$P_{u.KK.exp}$ (kN)	$P_{u.TW.num.F}$ (kN)	$P_{u.KK.num}$ (kN)	$P_{u.TW.num.R}$ (kN)	$\frac{P_{u.TW.num.F}}{P_{u.KK.exp}}$	$\frac{P_{u.TW.num.R}}{P_{u.KK.num}}$	$\frac{P_{u.KK.num}}{P_{u.KK.exp}}$
120(1)	285	101.9	101.9	108.8	103.6	1.000	0.952	1.067
120(2)	284	104.5	100.6	106.3	102.6	0.963	0.965	1.017
120(3)	283	100.5	104.4	108.7	106.0	1.039	0.975	1.082
140	285	104.0	106.1	110.5	109.3	1.020	0.989	1.063
140(1)	285	106.9	105.5	110.6	108.0	0.987	0.976	1.035

The observation of the results displayed in Figures 4.3(a)-(b) and Table 4.2 leads to the following conclusions:

(i) The numerical results obtained in this work for laterally free columns are in fairly good agreement with the experimental values reported by KUMAR & KALYANARAMAN (2014). Indeed, (i_1) it is clear that the numerical equilibrium paths obtained in this work follow quite closely the experimental ones and (i_2) the corresponding failure loads correlate rather well – the $P_{u.TW.num.F}/P_{u.KK.exp}$ values are comprised between *0.963* and *1.039*.

(ii) The numerical failure loads obtained in this work for laterally restrained columns also agree fairly well with those reported by KUMAR & KALYANARAMAN (2014), even if all the $P_{u.TW.num.R}/P_{u.KK.num}$ values are slightly below *1.00* – they are comprised between *0.952* and *0.989*.

(iii) On the basis of the comparisons made in the previous items, it seems fair argue that the shell finite element model employed in this work may be deemed as adequately validated.

(iv) It is interesting to notice that all numerical failure loads obtained for the restrained columns, either in this work or by KUMAR & KALYANARAMAN, overestimate the experimental values. This overestimation is more pronounced in the latter case, as the values of the ratio $P_{u.KK.num}/P_{u.KK.exp}$ are comprised between *1.017* and *1.082*. The decision to perform numerical simulations of the experimental tests, in which the specimens were laterally free, using a model with the column laterally restrained (displacements associated with minor-axis flexure prevented) is questionable - this issue will be addressed next.

Concerning the use of the additional lateral support in the numerical analysis, Figures. 4.4(a)-(b) display the equilibrium paths $P/P_{cr.D}$ *vs.* $|\delta|/t$ concerning columns SLC140(1) and SLC120(3) (see Table 3.1), both simulating experimental tests with the rigid-body in-plane translations and torsional rotations either free or fully prevented. It is observed that the two pairs of equilibrium paths only differ in the fairly close vicinity of the failure load. Nevertheless, it is clear that the additional support conditions increase the column distortional failure loads – recall that KUMAR & KALYANARAMAN reported that their numerical simulations overestimated the experimental distortional failure loads by an amount varying between *1.6*% and *12.2*%. The numerical simulations performed in this work showed differences comprised between *1.3*% and *3.9*% (see Table 4.2). It is still interesting to point out that the additional support conditions have a slightly larger influence on the distortional post-buckling behaviour of PLC[10] in Figure 4.5 for column PLC85(1) (see Table 3.2) – note that the restrained column equilibrium path is always visibly (but marginally) above its free column counterpart.

[10] Reported by SANTOS *et. al.* (2014).

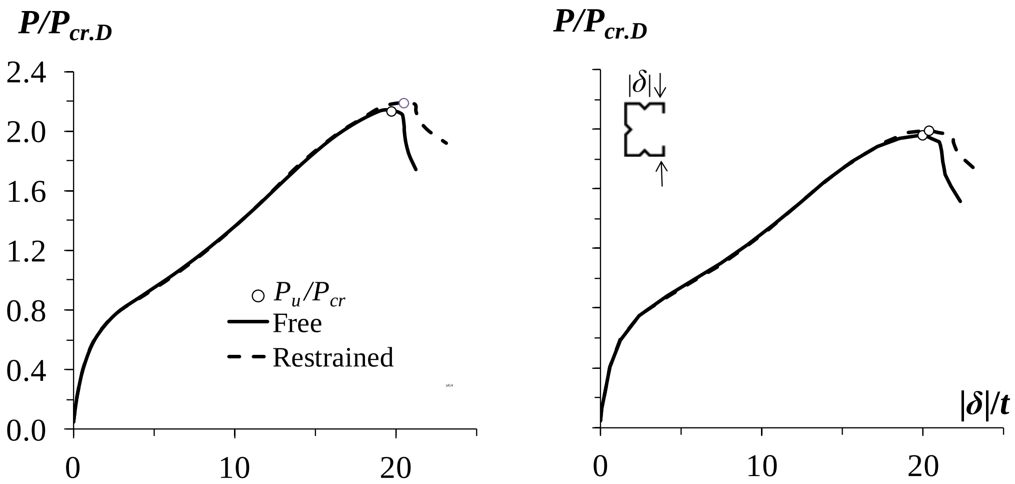

(a) (b)

Figure 4.4. Equilibrium paths of (a) SLC 140(1) and (b) SLC 120(3) columns with and without the additional support conditions.

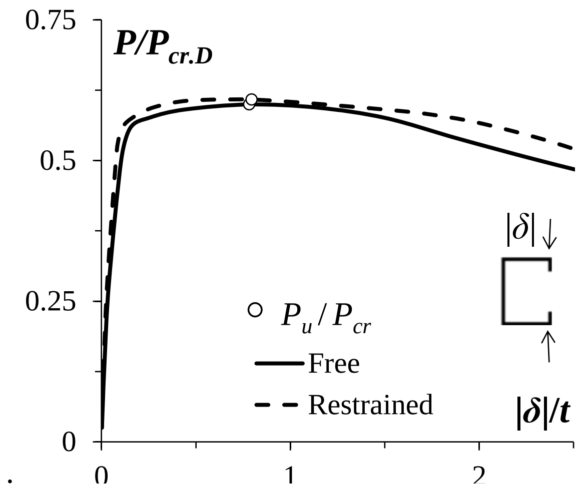

Figure 4.5. Equilibrium paths of PLC85(1) columns with and without the additional support conditions.

5 Post-buckling, Ultimate Strength and DSM

This chapter presents and discusses the results obtained from numerical elastic and elastic-plastic post-buckling analysis of SLC columns, performed through ANSYS. Item 5.1 presents the elastic post-buckling results. The elastic-plastic post-buckling behaviour and ultimate strength are presented in item 5.2. The item 5.3 addresses the DSM, comparing ultimate strength results obtained in this work to the DSM prediction and the influence of modal participation in the ultimate strength.

5.1 Elastic post-buckling behaviour

An elastic post-buckling analysis were performed in order to verify which flange-lip motion (inward or outward) leads the column to the lower stiffer condition and also to assess how the column elastic distortional post-buckling behaviour is influenced by the V-shaped intermediate stiffeners. Obviously, the distinction between outward and inward flange-stiffener motions is only relevant when the column critical buckling mode involves an odd number of half-waves.

Following the column distortional post-buckling asymmetry behaviour reported by SILVESTRE & CAMOTIM (2006), the initial imperfections involving inward flange-lip joint motions led all columns analyzed to the lower post-buckling strengths. Figure 5.1 exemplifies this assertion presenting the elastic equilibrium-path for SLC-75(1)-100(1). These equilibrium paths plot the applied load normalized ($P/P_{cr.D}$) values against the normalized displacement $|\delta|/t$, where $|\delta|$ is the maximum absolute transversal displacement occurring along the flange-lip longitudinal edges and t is the wall thickness.

In order to illustrate the elastic post-buckling equilibrium paths obtained and address the qualitative and quantitative assessment of how the column elastic distortional post-buckling behaviour is influenced by the V-shaped intermediate stiffeners, Figure 5.2 shows the post-buckling equilibrium paths of the *9* columns dealt with in this work (given by Tables 3.1 and 3.2). The observation of these sets of distortional post-buckling equilibrium paths prompts the following remarks:

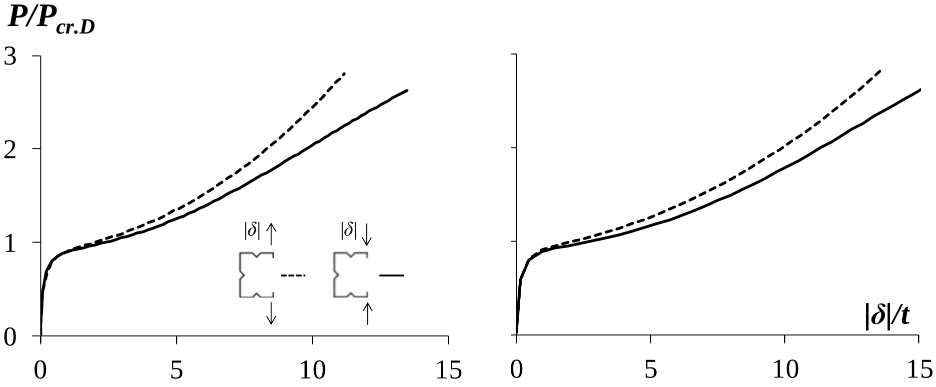

(a) (b)

Figure 5.1. Elastic equilibrium paths $P/P_{cr.D}$ vs. $|\delta|/t$ concerning (a) SLC75(1) and (b) SLC100(1) columns.

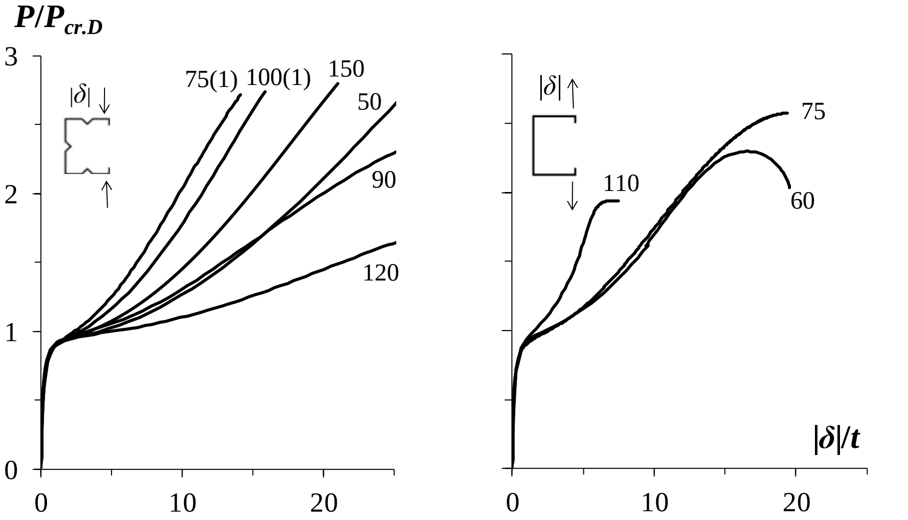

(a) (b)

Figure 5.2. Elastic equilibrium paths $P/P_{cr.D}$ *vs.* $|\delta|/t$concerning (a) SLC and (b) PLC columns.

(i) First of all, it can be noticed a wide variety of behavioural features exhibited by the $P/P_{cr.D}$ *vs.* $|\delta|/t$ curves concerning the columns analyzed, which means that the joint influence of the cross-section dimensions and presence of the V-stiffeners on the column elastic distortional post-buckling behaviour is quite complex and deserves further investigation. Moreover, there is also a clear difference between the SLC columns and PLC columns equilibrium path shapes (Figure 5.2 (a) and (b)): while the latter exhibit a pronounced convexity, which is associated with progressive stiffness degradation that leads to elastic limit points (visible in the PLC columns), the former display a concavity, which stems from the stiffness increase provided by the V-stiffeners and precludes the occurrence of an elastic limit point (at least for an acceptable, *i.e.*, not too high displacement value), which implies that the "ductility" prior to failure is also influenced considerably by the presence of V-stiffeners.

(ii) The comparison between sets of plots in Figure 5.2 shows that there is no clear evidence concerning the correlation of the web-to-flange width ratio (*h/b*) with the post-critical strength. The only exception is the PLC columns (Figure 5.2(b)) – one notice that since the PLC60 and PLC75 columns share the same web-to-flange width ratio (*h*/*b* equal to *1.0*), their elastic equilibrium paths are almost perfectly coincident. On the other hand, the PLC110 column (*h/b* equal to *1.83*) exhibits higher post critical dispersion. In fact, as previously stated by LANDESMANN *et al*. (2013), the elastic post-critical strength generally increases with *h/b*.

(iii) In spite of its limited scope (only *23* SLC columns analyzed), this study makes it possible to anticipate that both the cross-section dimensions and presence of V-stiffeners are bound to affect considerably the characteristics of the column elastic distortional post-buckling stiffness and strength, which may have non-negligible implications on the corresponding (elastic-plastic) ultimate strength and, therefore, on its prediction by design methods.

5.2 Elastic-plastic post-buckling behaviour and ultimate strength

The aim of this Section is to present and discuss the ultimate strength data gathered from the parametric study carried out in ANSYS finite element model, previously validated in Section 4.2.

In order to complement the failure load set considered by KUMAR & KALYANARAMAN (2014) and overcome its limitations, this Section includes a numerical (ANSYS SFEA) parametric study involving *155* SLC columns and aimed at obtaining a more representative distortional failure load data bank – in particular, the columns analyzed exhibit (i) web-to-lip width ratios ranging from *6.67* to *26.84* and (ii) distortional slenderness[11] values varying between *0.62* to *3*.69. Tables A1 to A4, included in Appendix A, provide the SLC column (i) yield stresses f_y, (ii) squash loads P_y, (iii) λ_D values, (iv) failure loads P_u and associated limit $|\delta|/t$ values, denoted $(|\delta|/t)_{\text{lim}}$,

[11] Recall that $\lambda_D = [P_y / P_{cr.D}]^{0.5}$, where $P_y = A \cdot f_y$ and A is the cross-section area.

and (v) ultimate load ratios $P_u/P_{cr.D}$ and P_u/P_y. Then, the extended SLC distortional failure load set, comprising the numerical values obtained in this work and the experimental and numerical values reported by KUMAR & KALYANARAMAN, is used to assess the merits of the DSM distortional strength curve newly proposed by these authors.

Figure 5.3 (a)-(b) display samples of the non-linear (geometrically and materially) equilibrium paths $P/P_{cr.D}$ *vs.* $|\delta|/t$ determined to obtain the ultimate loads P_u (identified by white circles) - these equilibrium paths concern SLC120 and PLC60 columns with f_y*=250-550-700-750-1200MPa* (in the figure *S250* is the equilibrium path for f_y*=250MPa* and so on). The elastic equilibrium paths, already shown in Figure 5.2 (a)-(b), are presented again for comparison purposes. Moreover, the column deformed configurations, in the close vicinity of failure (f_y*=750MPa* for SLC120 and f_y*=700MPa* for PLC60) are also presented - the column collapse distortional nature is clearly shown.

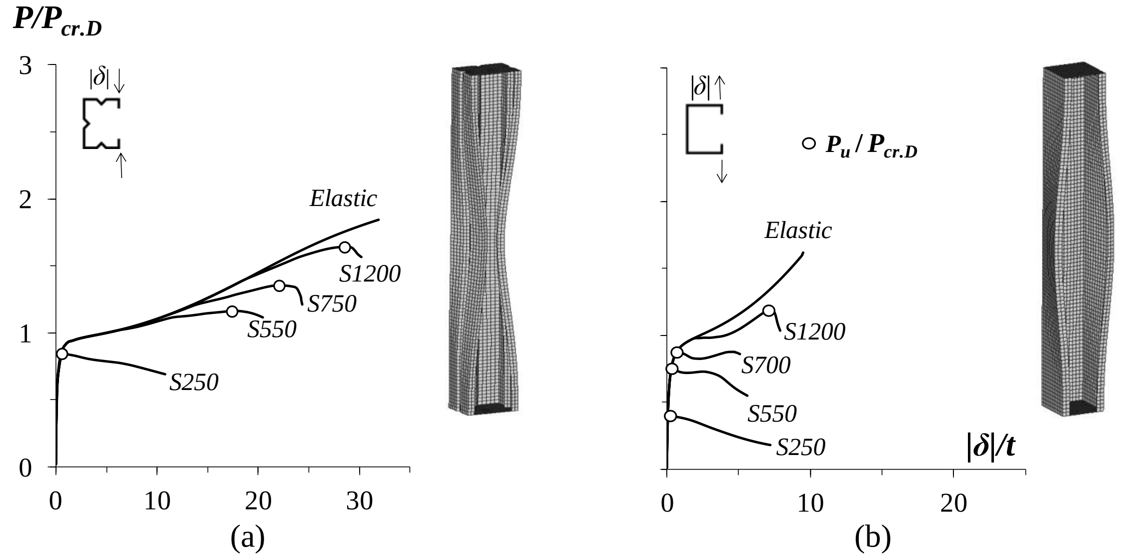

Figure 5.3. Distortional elastic-plastic pathway ($P/P_{cr.D}$*vs.*$|\delta|/t$) of (a) SLC120 and (b) PLC60 columns with f_y*=250-550-700-750-1200MPa*.

The observation of the results shown in the above figures, as well as the data provided in Tables A1 to A4 (see Appendix A), leads to the following conclusions:

(i) As expected, the ultimate load ratios $P_u/P_{cr.D}$ and associated $(|\delta|/t)_{\lim}$ values increase with the yield stresses f_y, regardless of the cross-section dimensions and presence (or not) of V-stiffener.

(ii) All columns exhibit single half-wave distortional buckling and failure modes, however, as mentioned previously, with distinct mid-span flange-lip motions: outward for PLC columns and inward for SLC columns.

Figures 5.4(a)-(c), concern SLC100-120 and PLC60 columns with f_y*=750MPa* (for SLC) and f_y*=700MPa* (for PLC), display their elastic-plastic equilibrium paths and the evolution of their deformed configurations[12] and *von Mises* stress contours (before, at and beyond the peak load) - the *5* diagrams correspond to the equilibrium states indicated on the equilibrium path. It is worth noting that (i) the deformed configurations are amplified *3* times, and that (ii) state *III* always corresponds to the column collapse. The observation of these results prompts the following remarks:

(i) The columns exhibit single half-wave distortional buckling and failure modes with inward mid-span flange-lip motions for SLC columns.

(ii) It can be observed that collapse in SLC columns are similar and start at de mid-span zone – see diagram *II* – associated with the yielding of the web-flange junction leading to the formation of a "distortional plastic ringe" – see diagram *III*.

(iii) In PLC column, the diagram *III* reveals that the yielding occurs in the lip at mid-span.

Figures 5.5(a)-(b) provide the failure load ratios $P_u/P_{cr.D}$ (Figure 5.5(a)) and P_u/P_y (Figure 5.5 (b)) against the distortional slenderness λ_D for the SLC columns (i) tested by KUMAR & KALYANARAMAN (2014) ($KK._{exp}$), (ii) numerically analyzed by these authors ($KK._{num}$) and (iii) numerically analyzed in this work ($TW._{num.}$). In order to assess the influence of the web-to-lip width ratio (h/d), the $P_u/P_{cr.D}$ and P_u/P_y values obtained in this work are identified by (i) white circles, for $h/d \geq 20$, (ii) grey diamonds, for $9 < h/d < 20$, and (iii) white squares, for $h/d < 9$. Recall that the values reported by KUMAR & KALYANARAMAN concern columns with h/d values comprised between *12* and *27* ($h/d=20$ for all the numerical ones) – they are identified by black triangles (numerical) and circles (experimental). The observation of the results shown in Figures 5.5(a)-(b), as well as the data given in Appendix A, leads to the following conclusions:

[12] Taking advantage of the ANSYS features, at this point of the study all columns were inspected in the vicinity of the failure load to verify if any modal interaction occurred. No kind of interaction was noticed before - or at moment - the ultimate load was reached.

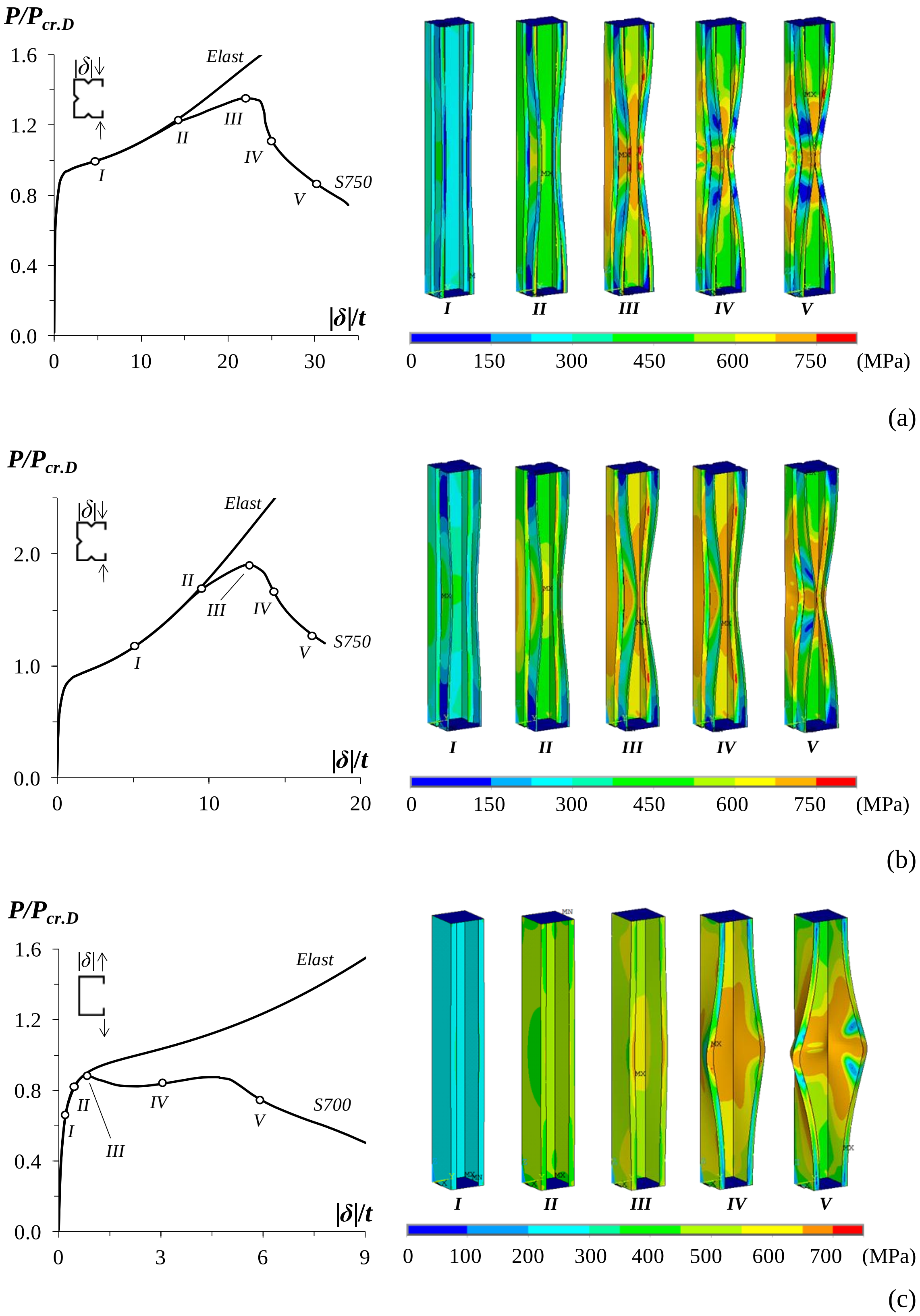

Figure 5.4. Elastic and elastic-plastic equilibrium paths, deformed configurations (including the collapse mechanism) and *von Mises* stress contours (f_y=750 *MPa*) for (a) SLC120, (b) SLC100(1) and (c) PLC60 columns (f_y=700 *MPa*).

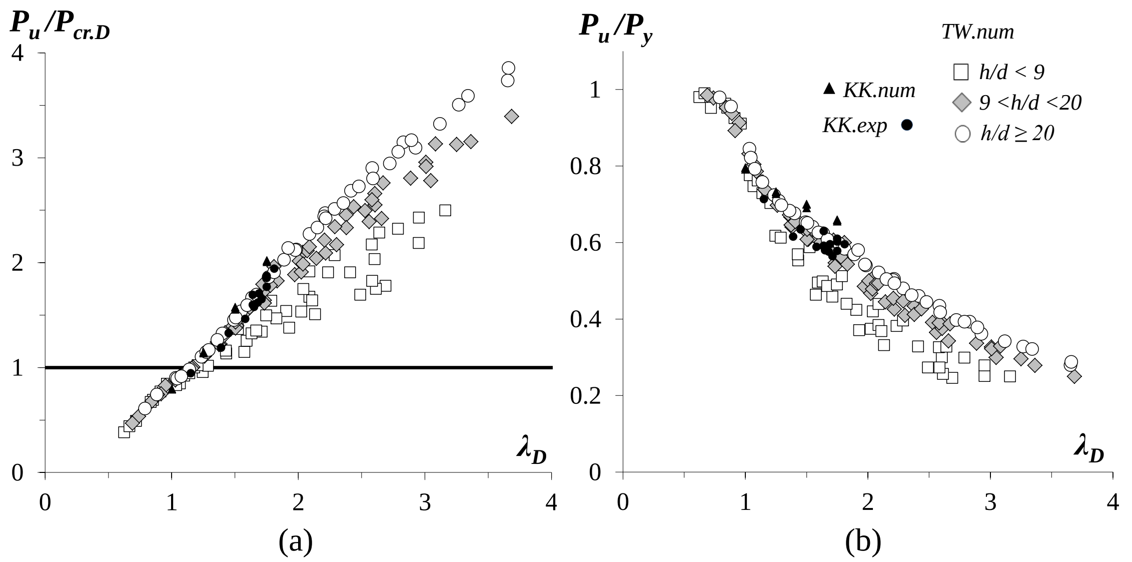

Figure 5.5. Plots of the ultimate load ratios (a) $P_u/P_{cr.D}$ and (b) P_u/P_y against the distortional slenderness λ_D.

(i) Figure 5.5(a) shows that, naturally, the failure load ratios $P_u\ /P_{cr.D}$ of the SLC columns analyzed (in this work and by KUMAR & KALYANARAMAN) increase with the distortional slenderness λ_D - note that $P_u/P_{cr.D} > 1$ for λ_D larger than approximately *1.1*. The variation $P_u\ /P_{cr.D}$ *vs.* λ_D is fairly linear and, for $\lambda_D > 1.5$, it is noticeable that the slope increases with h/d – in particular, the values concerning the columns with $h/d < 9$ visibly and consistently deviate ("down") from the remaining ones.

(ii) As expected, the P_u/P_y *vs.* λ_D "cloud" depicted in Figure 5.5(b) follows the general trend of a "Winter-type" strength/design curve. However, a considerably P_u/P_y "vertical dispersion" is observed, particularly in the high slenderness range – indeed, the P_u/P_y values only exhibit a small vertical dispersion for λ_D lower than about *1.25*. Moreover, like for the $P_u\ /P_{cr.D}$ ratios, there is again a very clear influence of h/d on the P_u/P_y values. Indeed, this geometric ratio is the main "culprit" for the aforementioned vertical dispersion for the present set of cross-sections – for a given (high) λ_D value, P_u/P_y clearly decreases with h/d.

(iii) It is very clear that the set of experimental and numerical (mostly) results reported by KUMAR & KALYANARAMAN is insufficient to draw meaningful conclusions concerning the DSM design of SLC columns failing in distortional modes. In fact, as already mentioned, they (iii$_1$) cover only the *1.00-1.81* slenderness interval and (iii$_2$) exhibit mostly h/d ratios either in close vicinity or above *20* (the value shared by all the columns analyzed numerically).

(iv) One notice that the P_u/P_y values for $\lambda_D \geq 1.25$ present some vertical dispersion and they are ordered according to its h/d ratio in the following sequence (higher to lower values): $h/d \geq 20$, $9<h/d<20$ and $h/d<9$ – this sequence is more perceptible for $\lambda_D \geq 1.5$. In addition, for almost all SLC columns the joint contribution of local deformations modes **7** and **9** ($\boldsymbol{p_{7+9}}$) are also in the same sequence. The average participation of $\boldsymbol{p_{7+9}}$ for the range of h/d ratio is: *18.82%* for $h/d \geq 20$, *8.17%* for $9<h/d<20$ and *4.26%* for $h/d<9$. Thus, based on this limited amount of results, it seems fair to conclude that the participation of local mode deformations - associated to h/d ratio - may influence the post-critical strength of SLC columns.

In the next Section, the failure load data bank presented and discussed is used to assess the DSM design of SLC columns against distortional failures.

5.3 Direct Strength Method

The adequacy of the currently codified DSM distortional design curve, named here as DSM-D and given by Equation 5.1 to estimate SLC column failure loads is now addressed, devoting particular attention to the comparison between its predictions and those provided by the alternative strength curve recently proposed by KUMAR & KALYANARAMAN (2014) – the DSM-DP curve, defined by Equation 5.2. Note that the two design expressions, its curves were already displayed in Figure 2.20, exhibit the same format and only differ in the three coefficients.

$$P_{n.D} = \begin{cases} P_y & \text{for } \lambda_D \leq 0.561 \\ P_y\left[1-0.25\left(P_{cr.D}/P_y\right)^{0.6}\right]\left(P_{cr.D}/P_y\right)^{0.6} & \text{for } \lambda_D > 0.561 \end{cases} \qquad \text{(Eq. 5.1)}$$

$$P_{n.DP} = \begin{cases} P_y & \text{for } \lambda_D \leq 0.474 \\ P_y\left[1-0.23\left(P_{cr.D}/P_y\right)^{0.3}\right]\left(P_{cr.D}/P_y\right)^{0.3} & \text{for } \lambda_D > 0.474 \end{cases} \qquad \text{(Eq. 5.2)}$$

Figures 5.6(a)-(b) compares the both the DSM-D and DSM-DP strength curves with the failure load ratios P_u/P_y concerning the SLC columns (i) experimentally ($P_{u.KK.exp}$) and numerically ($P_{u.KK.num}$) analyzed and by KUMAR & KALYANARAMAN (Figure 5.6(a)) and (ii) numerically analyzed in this work (Figure 5.6(b)) – the latter are separated according to their h/d ratios. On the other hand, Figure 5.7(a)-(b) plot those same $P_u\ /P_{n.D}$ and $P_u\ /P_{n.DP}$ ratios against λ_D, thus providing pictorial representations of the accuracy and safety associated with the two design curves under consideration – the averages, standard deviations and maximum/minimum values of the $P_u\ /P_{n.D}$ or $P_u\ /P_{n.DP}$ ratios included in each plot are also given. The analysis of these design results leads to the following comments:

(i) First of all, the observation of Figures 5.6(a) and 5.7(a_1) provides very clear evidence on why KUMAR & KALYANARAMAN (2014) proposed the DSM-DP design curve: it fits their *26* experimental and numerical failure loads almost perfectly. Indeed, the corresponding $P_u\ /P_{n.DP}$ indicators are *1.02* (average), *0.06* (standard deviation), *1.11* (maximum value) and *0.92* (minimum value). Moreover, Figures 5.6(a) and 5.7(b_1) show that the current DSM-D design curve yields extremely conservative predictions of these same failure load set, as reflected by the respective indicators $P_u/P_{n.D}$: *1.26* (average), *0.13* (standard deviation), *1.48* (maximum value) and *1.06* (minimum value).

(ii) However, the comparison between Figures 5.6(b) and 5.7(a_2) provides evidence on how premature and ill-advised was to propose a new strength curve on the basis of such a small and "biased" set of failure loads. In fact, when the pool of SLC failure loads is enlarged, both in column cross-section geometries and slenderness values, the inadequacy of the DSM-DP design curve becomes more clear: the indicators $P_u/P_{n.DP}$ concerning the SLC column failure loads numerically obtained in this work[13] are *0.89* (average), *0.16* (standard deviation), *1.18* (maximum value) and *0.51* (minimum value), *i.e.*, surely inadequate, particularly for columns with small h/d ratios and/or large slenderness values.

(iii) Concerning the ultimate numerical results obtained in this work, the DSM-D estimates are (iii_1) mostly safe and conservative in the small-to-moderate

[13] Note that several column geometries considered by KUMAR & KALYANARAMAN (2014) were also dealt with in this work. But, by adopting higher yield stresses, it was possible to cover with them wider slenderness ranges.

slenderness range ($\lambda_D \leq 1.25$) and (iii$_2$) quite conservative for columns in the moderate-to-high slenderness range ($\lambda_D \geq 1.25$) – the difference between $P_{u.TW.num.F}$ and the DSM-D prediction tends to grow when the web-to-lip ratio (h/d) increases and is clearly visible for columns with $h/d \geq 20$, which are reflected in the $P_u/P_{n.D}$ ratios. Therefore, it is clear that web-to-lip ratio adopted seems to influence visibly the $P_u/P_{n.D}$ and $P_u/P_{n.DP}$ "distributions" displayed in Figure 5.7(a$_2$)(b$_2$), whose averages, standard deviations and maximum/minimum values are provided.

(iv) The DSM-D estimates of the SLC columns ultimate loads (experimentally or numerically) reported by KUMAR & KALYANARAMAN are on the safe side for both the experimental and (mostly) numerical results. However, one recalls that these results (ii$_1$) concern SLC columns with a quite limited (small-to-moderate) distortional slenderness range, comprised between *1.0* and *1.81*, and (ii$_2$) exhibit web-to-lip ratio between *12.7* and *26.8* – all (*12*) numerical analysis results concern columns with $h/d = 20$.

(v) However, it is fair to say that, after looking at Figures 5.6(b) and 5.7(b$_1$)-(b$_2$), it can be concluded that the DSM-D design curve underestimates (sometimes quite considerably) the failure loads of several columns, particularly those exhibiting large *h*/*d* ratios and/or small slenderness values[14].

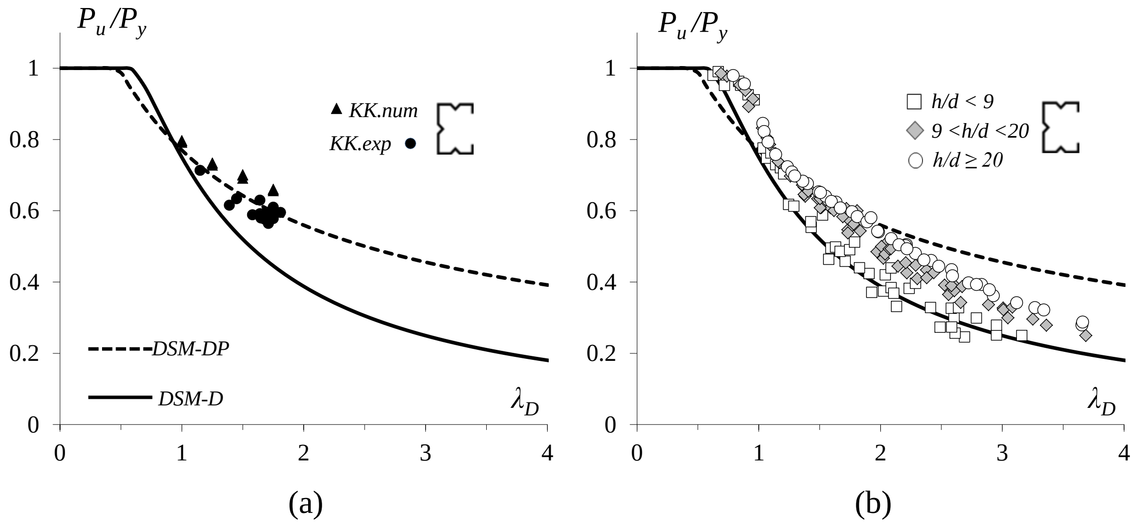

Figure 5.6. Comparison between the DSM-D and DSM-DP strength curves and the SLC column failure loads obtained (a) by KUMAR & KALYANARAMAN (2014) and (b) in this work.

[14] Recall that all the columns analyzed by KUMAR & KALYANARAMAN (2014) fall into this category.

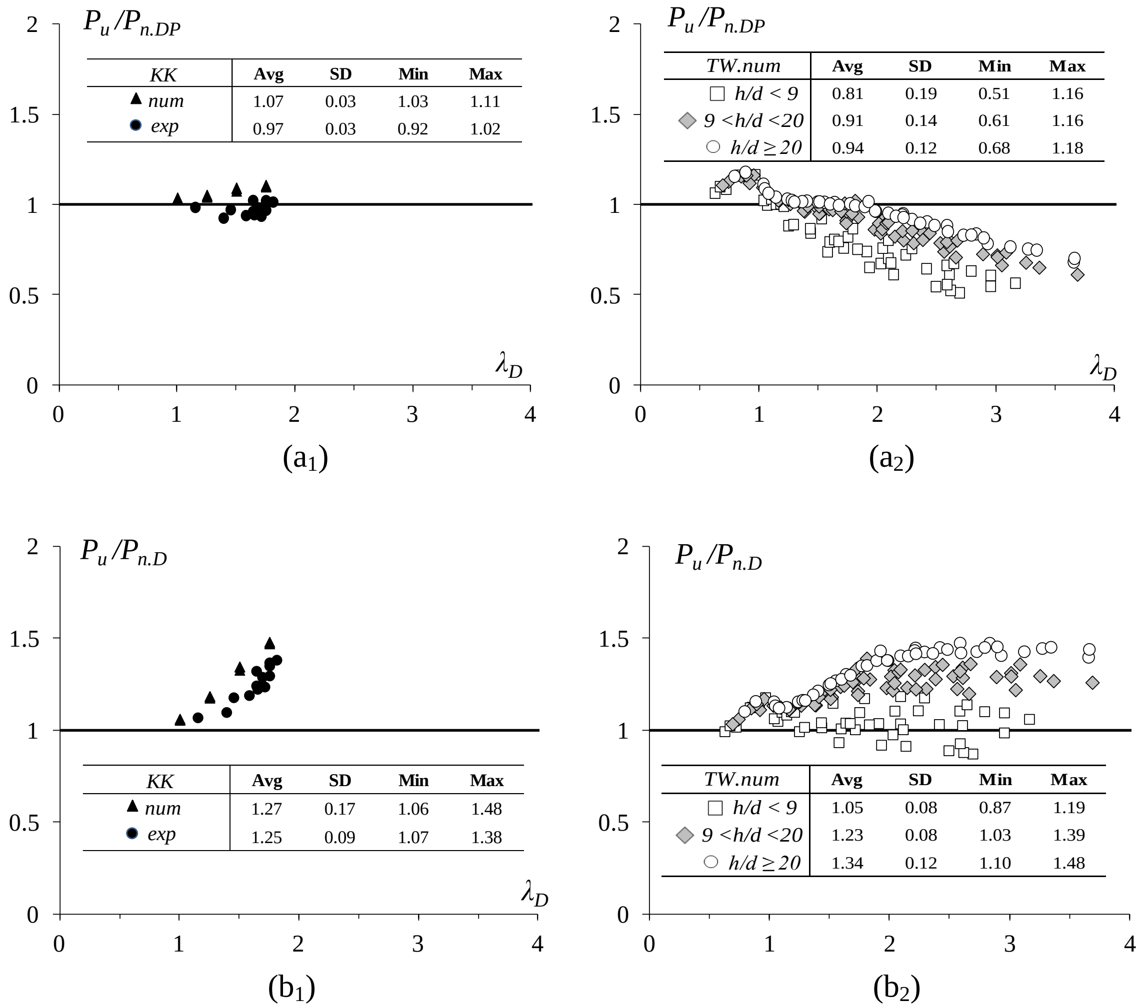

Figure 5.7. (a) $P_u /P_{n.DP}$ and (b) $P_u /P_{n.D}$ values and indicators concerning the SLC columns analyzed ($_1$) by KUMAR & KALYANARAMAN (2014) and ($_2$) in this work.

In order to enable a better assessment of the quality of the DSM-D design curve predictions, Figures 5.8(a)-(c) show results similar to those presented in Figures 5.6(b) and 5.7(b$_2$), respectively, for *20* PLC columns buckling and failing in distortional modes. These columns, which were previously numerically analyzed by LANDESMANN & CAMOTIM (2013) or SANTOS *et al.* (2014), have the geometries and material properties defined in Tables 3.2 and the yield stresses indicated in Table B1, included in Appendix B – these tables also provide the PLC column P_y, λ_D, P_u and $P_u/P_{n.D}$ values. The observation of the design results displayed in Figures 5.8(a)-(c) prompts the following remarks:

(i) As expected, the DSM-D design curve provides accurate and safe predictions of the numerical distortional loads, as attested by the corresponding $P_u/P_{n.D}$ values plotted in Figure 5.8(b).

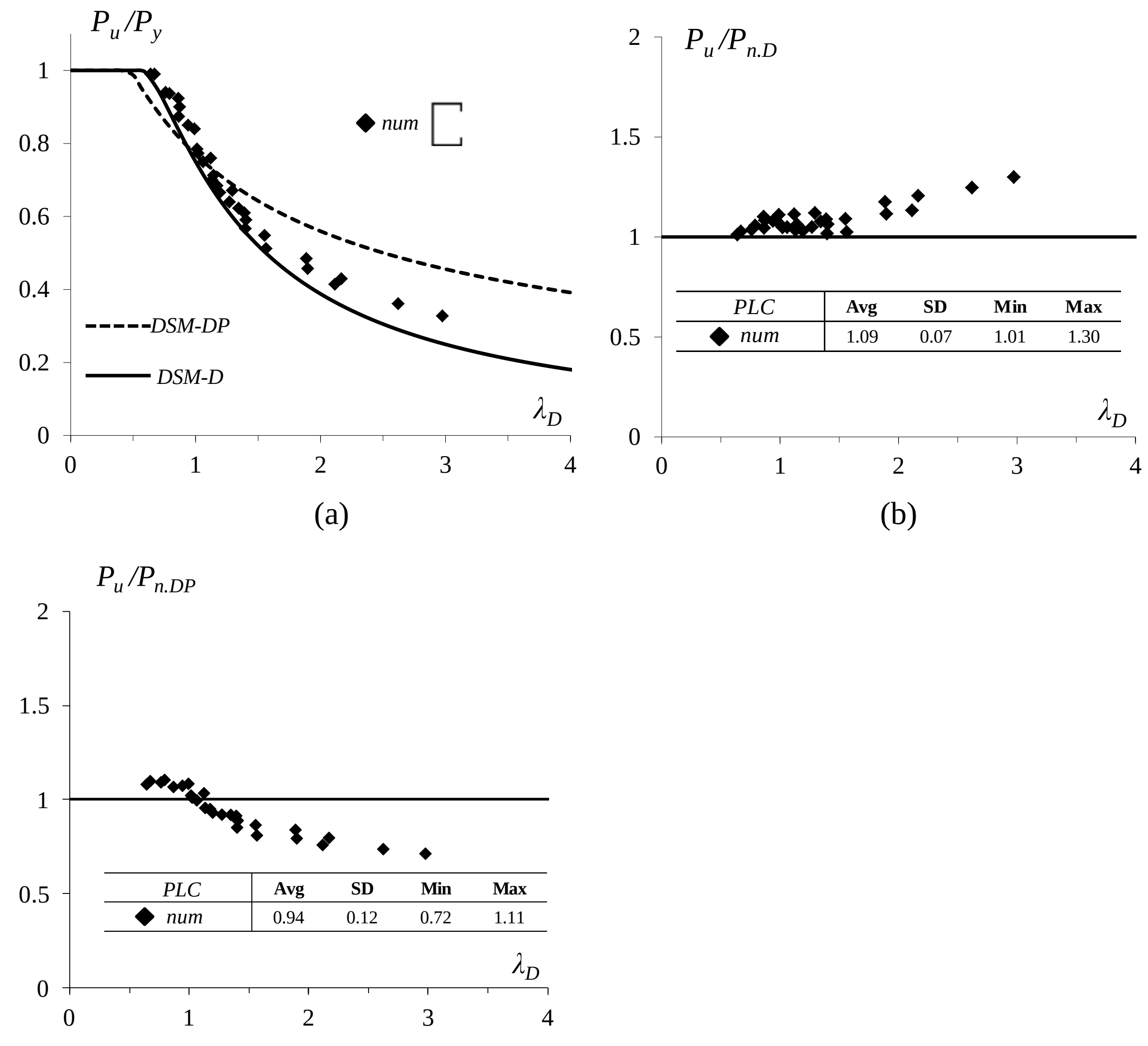

(c)

Figure 5.8. (a) Comparison between the DSM-D and DSM-DP strength curves and the PLC column failure loads obtained by LANDESMANN & CAMOTIM (2013) or SANTOS *et al.* (2014) and corresponding (b) $P_u / P_{n.D}$ and (c) $P_u / P_{n.DP}$ values and indicators.

(ii) Since the DSM-DP curve lies under the current one for slenderness $\lambda_D < 1$, approximately, the estimates are (ii$_1$) conservative for $\lambda_D<1$ and (ii$_2$) unsafe side in the higher slenderness range. The DSM-D estimates are (ii$_1$) safe and accurate for $\lambda_D \leq 1.5$ and (ii$_2$) on the safe side (but still fairly accurate) in the higher slenderness range – the underestimation tends to grow as λ_D increases, as can be attested by the predictions presented.

(iii) The DSM-DP strength curve provides unsafe ultimate load estimates for most of the columns analyzed – the averages of the $P_u / P_{n.DP}$ ratios values are (iii$_1$) *0.94* for PLC columns (reported), (iii$_2$) *1.02* for SLC (reported) and (iii$_3$) *0.89* for SLC (obtained). On the other hand, the averages of the $P_u /P_{n.D}$ values (current DSM curve) are clearly “safer”: they are (iii$_4$) *1.09* for PLC (reported), (iii$_5$) *1.26* for SLC (reported) and (iii$_6$) *1.21* for SLC (obtained).

The above comparisons show that the DSM-DP strength curve overestimates the vast majority of numerical SLC and PLC columns ultimate loads dealt in this work, beyond the distortional slenderness range covered by KUMAR & KALYANARAMAN. This fact provides clear evidences that the decision to propose of a new DSM distortional design curve seems clearly premature.

6 Concluding Remarks

Recently, KUMAR & KALYANARAMAN (2014) reported experimental and numerical results concerning fixed-ended SLC columns and, on the basis of their results, proposed a new DSM distortional strength curve which lies well above both the currently codified DSM distortional and local design curves. This quite surprising finding constitutes a significant break from the existing knowledge, which is widely accepted by the scientific community working with cold-formed steel structures, and provides the motivation of this thesis.

In order to assess the validity of the claims made by KUMAR & KALYANARAMAN, this work reported a numerical ANSYS SFEA investigation on the distortional buckling and post-buckling behaviour, ultimate strength and design of CFS columns concerned (i) fixed ends support conditions, (ii) web/flange-stiffened lipped channel (SLC) and (iii) centered compression load. In addition, this paper also evaluates the accuracy of the current Direct Strength Method (DSM) recommendations to predict ultimate strength obtained numerically. To reach this goal, *155* SLC columns were numerically analyzed in this work corresponding to a combination of (i) *23* geometries and (ii) several yield stress, chosen in order to cover a wide variety of slenderness.

The first step consisted of selecting several column geometries associated with “pure” distortional buckling and failure modes, which was ensured by having local and global critical buckling loads much higher than their distortional counterparts – this column set included the specimens tested by KUMAR & KALYANARAMAN. After selecting the SLC column cross-section dimensions and lengths the mechanical characterization of the distortional critical buckling modes in the SLC columns was addressed, through the in-depth inspection of the results provided by the GBT buckling analysis. Next, the proposed ANSYS SFEA was validated by replicating numerically and experimental results reported by KUMAR & KALYANARAMAN (2014) for SLC columns subjected to centered compression load. The numerical model was employed to perform geometrically and materially non-linear analysis of the selected SLC columns and also to confirm that the columns modeled buckled and collapsed distortionally. The numerical results obtained (equilibrium paths, failure loads and deformed configurations) were then presented, discussed and compared. Out of the various findings obtained in the course of this work, the following ones deserve to be specially mentioned:

(i) The P_u/P_y *vs.* λ_D "cloud" concerning the SLC columns ultimate loads was shown to follow trends that can be accurately described by "Winter-type" strength/design curve – experimental/numerical distortional failure loads for SLC and PLC available in the literature also followed a similar trend.

(ii) A considerably P_u/P_y "vertical dispersion" was observed, particularly in the high slenderness range due to a very clear influence of h/d. Indeed, this geometric ratio is the main "culprit" for the aforementioned vertical dispersion – for a given (high) λ_D value, P_u/P_y clearly decreases with h/d.

(iii) It is very clear that the set of experimental and numerical results reported by KUMAR & KALYANARAMAN was insufficient to draw meaningful conclusions concerning the DSM design of SLC columns failing in distortional modes. In fact, as already mentioned:

(iii_1) only *26* columns were analyzed, either experimentally or numerically, which covered a quite limited (small-to-moderate) distortional slenderness range: *1.00-1.81*,

(iii_2) they exhibit mostly h/d ratios either in close vicinity or above *20* (the value shared by all the columns analyzed numerically)

(iii_3) the columns analyzed numerically were laterally restrained which was not considered in the tests. Even if the restraints were shown not to affect much the failure loads, visible increases still occurred.

The questionable assumptions and/or limitations indicated previously in item (*iii*) provided ample evidence that the proposal of the novel DSM distortional strength curve for stiffened lipped channels was premature and ill-advised. Indeed, the failure load estimates yielded by this strength curve, for the *155* columns analyzed in this work and the *26* column analyzed by KUMAR & KALYANARAMAN, were shown to provide safe and accurate failure load predictions only in the low-to-moderate slenderness range ($\lambda_D \leq 1.25$). For more slender SLC columns, this curve generally yields quite large failure load overestimations, which grow as the web-to-lip width ratio decreases and/or the slenderness increases.

On the other hand, the analysis of the failure load predictions provided by the current DSM distortional design curve unveiled a rather different picture – in fact, it yields safe for the vast majority of the columns considered (only the failure loads of a few fairly slender columns with low *h*/*d* values were overestimated). However, these estimates were also found to become excessively safe as the column *h*/*d* value increases.

In summary, it can be concluded that the current DSM distortional design curve can continue to be used to estimate failure of web-flange stiffened cold-formed steel columns, even it provides fairly large overestimations for some column geometries – but not nearly as large as implied by the strength curve proposed by KUMAR & KALYANARAMAN (2014). If it is deemed useful by the scientific community dealing with cold-formed steel structures to develop a more refined DSM approach for this type of columns, the results obtained in this work provided evidence that such an approach should involve the web-to-lip width ratio (*h*/*d*) as a key parameter.

6.1 Suggestions for future works

The results obtained in this work provided strong evidences that the DSM strength curve proposed by KUMAR & KALYANARAMAN (2014) was precipitated and the current DSM curve for fixed-ended columns under distortional buckling can be used to ultimate load prediction of web-flange stiffened lipped channel (even though this specific cross-section was not considered in the DSM validation studies). However, new analysis may contribute to the present work - confirming, bringing other questionings or even refuting the conclusions presented here. Thus, the scope of the present investigation can be extended as follows:

(i) Choosing different, and maybe more complex, column geometries (cross-section shape/dimensions and lengths) giving special attention to the web-to-lip width ratio (*h/d*) influence on the modal participation and on the ultimate load.

(ii) Performing analysis considering others end support conditions (since there are some works that also claim a new DSM for different support conditions).

7 Bibliography

ABNT, 2010. *Brazilian Standard on Design of Cold-Formed Steel Structures* (NBR 14762:2010), Brazilian Standards Association, Rio de Janeiro, RJ. (Portuguese)

AISI, 2012. *North American Specification for the Design of Cold-Formed Steel Structural Members* (NAS), American Iron and Steel Institute, Washington DC.

AS/NZS, 2005. *Cold-Formed Steel Structures*, Standards of Australia (SA) and Standards of New Zealand (SNZ), Sydney-Wellington.

ANSYS, 2009. Reference Manual, *Swanson Analysis Systems* (*SAS*), version12.0.1

BASAGLIA C., CAMOTIM D., SILVESTRE N., 2011. "Non-linear GBT formulation for open-section thin-walled members with arbitrary support conditions", *Computers and Structures*, v.89, pp. 1906-1919.

BATISTA E.M., 2010. "Effective section method: A general direct method for the design of steel cold-formed members under local–global buckling interaction", *Thin-Walled Structures*, v.48, pp. 345-356.

BATISTA E.M., GHAVAMI K., 2005. "Development of Brazilian steel construction", *Journal of Constructional Steel Research*, v.61, pp. 1009-1024.

BEBIANO R., SILVESTRE N., CAMOTIM D., 2008. GBTul – A code for the buckling analysis of cold-formed steel members, *Proceedings of19th International Specialty Conference on Recent Research and Developments in Cold-Formed Steel Design and Construction* (St. Louis, 14-15/10), R LaBoube, W.-W. Yu (eds.), 61-79.

BEBIANO R., PINA P., SILVESTRE N., CAMOTIM D., 2010a. *GBTUL 1.0β – Buckling and Vibration Analysis of Thin-Walled Members*, DECivil/IST, Technical University of Lisbon. (http://www.civil.ist.utl.pt/gbt)

BEBIANO R., PINA P., SILVESTRE N., CAMOTIM D., 2010b. *Manual user.GBTUL 1.0β – Buckling and Vibration Analysis of Thin-Walled Members*, DECivil/IST, Technical University of Lisbon. (http://www.civil.ist.utl.pt/gbt)

CSSBI – Canadian Sheet Steel Building Institute. Lightweight Steel Framing, Photo Gallery. http://www.cssbi.ca/products/commercial/lightweight-steel-framing/photo-gallery. Acessed on September 15, 2014.

DINIS P.B., CAMOTIM D., 2010. "Local/distortional mode interaction in cold-formed steel lipped channel beams", *Thin-Walled Structures*, v.48, pp.771–785.

DINIS P.B., BATISTA E.M., CAMOTIM D., SANTOS E.S., 2012. "Local-distortional-global interaction in lipped channel columns: experimental results, numerical simulations and design considerations", *Thin-Walled Structures*, v.61, pp.2-13.

DINIS P.B., YOUNG B., CAMOTIM D., 2014. "Strength, interactive failure and design of web-stiffened lipped channel columns exhibiting distortional buckling", *Thin-Walled Structures*. v.81, pp.195-209.

DNA NACIONAL - http://www.dnanacional.com.br/ . Accessed on October 16, 2014.

DON ALLEN, P.E., 2006. Structure Magazine, November. http://www.structuremag.org/wp-content/uploads/2014/09/C-BB-History-AllenLowndes-Nov061.pdf. Accessed on September 15, 2014.

EL-SHEIKH A.I., EL-KASSAS E.M.A., MACKIE R.I., 2001. "Performance of stiffened and unstiffened cold-formed channel members in axial compression", *Engineering Structures*, v.23, p.1221-1231.

ENCON - Encon Insulation. http://www.encon.co.uk/products/view/648/hadley-building-products-c-stud-53mc. Acessed on January 6, 2015

EUROCODE 3, 1993. *Design of steel structures - Part 1-3: General rules - Supplementary rules for cold-formed members and sheeting* (EN 1993-1-3), European Standard.

GARCIA R.A.S., LANDESMANN A., CAMOTIM D., 2014. "Distortional buckling, post-buckling and failure of cold-formed steel stiffened lipped channel columns", *Proceedings of the XXXVI South-American Structural Engineering Congress* (Montevideo, 19-21 /11). (Portuguese)

HAIDARALI M.R., NETHERCOT D.A., 2012. "Local and distortional buckling of cold-formed steel beams with both edge and intermediate stiffeners in their compression flanges", *Thin-Walled Structures*, v.54, pp. 106-112.

HANCOCK, G.J., KWON, Y.B., BERNARD, E.S., 1994. "Strength design curves for thin-walled sections undergoing distortional buckling", *Journal Construction*, v.31, pp. 169-186.

HANCOCK, G.J., MURRAY, T.M., ELLIFRITT, D.S., 2001. *Cold-formed Steel Structures to the AISI Specification*, Marcel Dekker, New York.

HANCOCK, G.J., 2003. "Cold-formed steel structures", *Journal of Constructional Steel Research*, v.59, pp.473-487.

HOON K.H., RHODES J., SEAH L.K., 1993. "Tests on intermediately stiffened plate elements and beam compression elements", *Thin-Walled Structures* v.16, pp.111-143.

IYENGAR, N.G.R., 1986. *Structural stability of columns and plates*, East-West Press PVT, New Delhi.

KUMAR, M.V., KALYANARAMAN V., 2012. "Design strength of locally buckling stub lipped channel columns", *Journal of Structural Engineering* (ASCE), v.138(11), pp.1291-1299.

KUMAR, M.V., KALYANARAMAN V., 2014. "Distortional buckling of CFS stiffened lipped channel compression members", *Journal of Structural Engineering (ASCE)*, 140(12), 04014099(14).

KWON Y.B., HANCOCK, G.J., 1992. "Tests of cold-formed channels with local and distortional buckling", *Journal of Structural Engineering.* v.117(7), pp. 1786-1803.

LANDESMANN, A., CAMOTIM, D., 2011. "DSM design of cold-formed steel columns against distortional failure: numerical investigation on the influence of the cross-section geometry and support conditions", *Proceedings of the Annual Stability Conference Structural Stability Research Council Pittsburgh, Pennsylvania, May 10-14, 2011*

LANDESMANN, A., CAMOTIM, D., 2013. "On the Direct Strength Method (DSM) design of cold-formed steel columns against distortional failure", *Thin-walled Structures*, v.67, pp. 168-187.

LANDESMANN, A., CAMOTIM, D., BASAGLIA, C., 2013. "Distortional Post-Buckling Behavior and Strength of Cold-Formed Steel Columns: How does the Cross-Section Geometry Affect it?", *Proceedings of the Annual Stability Conference Structural Stability Research Council St. Louis, Missouri, April 16-20, 2013*

LAU, S.C.W., HANCOCK, G.J., 1987. "Distortional buckling formulas for channel columns", *Journal of Structural Engineering*, v.113(5), pp. 1063-1078.

METFORM, 2014. *Steel Deck Technical Manual* – http://www.metform.com.br/telha-forma-catalogo-tecnico.php. Accessed on October 16, 2014. (Portuguese)

REIS, A., CAMOTIM, D., 2001. *Strucutral Stability*. McGraw-Hill. (Portuguese)

SANTOS E.S., BATISTA E.M., CAMOTIM D., 2012. "Experimental investigation concerning lipped channel columns undergoing local–distortional–global buckling mode interaction", *Thin-Walled Structures*, v.54, pp. 19-34.

SANTOS W.S., LANDESMANN A., CAMOTIM D., 2014. "Application of the DSM design of pin-ended cold-formed steel columns that buckle and failure in distortional mode", *Proceedings of the XXXV Iberian Latin American Congress on Computational Methods in Engineering* (Cilamce 2014 – Fortaleza, 23-26/11). (full paper in Cd-Rom Proceedings – Paper 0573). (Portuguese).

SCHAFER, B.W., 2000. *Distortional Buckling of Cold-formed Steel Columns*. The American Iron and Steel Institute (AISI) Final report, August 2000. http://www.ce.jhu.edu/bschafer/dist_columns/col-dist-rpt.pdf. Accessed on March 31, 2015.

SCHAFER, B.W., 2002. "Local, Distortional, and Euler buckling of thin-walled columns", *Journal of Structural Engineering*, v.128(3), pp. 289-299.

SCHAFER, B.W., 2008. "Review: The Direct Strength Method of cold-formed steel member design", *Journal of Constructional Steel Research*, v.64, pp.766-778.

SCHAFER, B.W., PEKÖZ, T., 1997. “The behavior and design of longitudinally stiffened thin-walled compression elements”, *Thin-Walled Structures*, v.27(1), pp. 65-78.

SCHAFER, B.W., PEKÖZ, T., 1998. “Direct strength prediction of cold-formed steel members using numerical elastic buckling solutions”, *Fourteenth International Specialty Conference on Cold-Formed Steel Structures*. St. Louis, Missouri, October 15-16.

SILVESTRE N., BEBIANO R., CAMOTIM D., 2005. “On the distortional post-buckling asymmetry of cold-formed steel channel columns with different stiffener configurations”, *Proceedings of the Annual Stability Conference Structural Stability Research Council Montreal, Quebec, 2005.*

SILVESTRE, N., CAMOTIM, D., 2006. “Local-plate and distortional post-buckling behavior of cold-formed steel lipped channel columns with intermediate stiffeners”. *Journal of Structural Engineering*, v.132(4), pp. 529-540.

SILVESTRE N., CAMOTIM D., DINIS P.B., 2012. “Post-buckling behaviour and direct strength design of lipped channel columns experiencing local/distortional interaction”, *Journal of Constructional Steel Research*, v.73, pp.12-30.

STRATCO, 2015. http://stratco.com.au/Products/Steel_Framing/Steel_Framing.asp. Accessed on January 5, 2015.

YANG D., HANCOCK G.J., 2003. *Compression tests of cold-reduced high strength steel channel columns failing in the distortional mode*. The University of Sydney, Department of Civil Engineering, Research Report nº R825.

YANG D., HANCOCK G.J., 2004. “Compression tests of high strength steel channel columns with interaction between local and distortional buckling**”,** *Journal of Structural Engineering*, v.130(12), pp.1954-1963.

YANG D., HANCOCK G.J., 2006. “Numerical simulation of high strength steel lipped channel columns”, *Advances in Steel Structures*, v.I, pp 149-154.

YAP, D.C.Y., HANCOCK, G.J., 2011. “Experimental study of high-strength cold-formed stiffened C-sections in compression”, *Journal of Structural Engineering*, v.137(2), pp. 162-172.

ZIEMIAN, R.D., 2010. *Guide to Stability Design Criteria for Metal Structures*, 6th Edition, John Wiley & Sons, New York.

APPENDIX A

Data concerning SLC columns

Tables A1 to A4 provide, for each SLC column analyzed in this work, the (i) yield stress f_y, (ii) squash load P_y, (iii) distortional slenderness λ_D, (iv) distortional failure load P_u and associated $(|\delta|/t)_{\mathrm{lim}}$ value, (v) failure load ratios $P_u/P_{cr.D}$ and P_u/P_y, (vi) DSM distortional failure load estimates $P_{n.D}$ and (vii) ratios $P_y/P_{n.D}$ and $P_u/P_{n.D}$.

Table A1: Numerical distortional failure loads and DSM estimates for the SLC 50-50(1)-50(2)-65-65(1) columns analyzed.

SLC	f_y (MPa)	P_y (kN)	λ_D	P_u (kN)	$(\lvert\delta\rvert/t)_{\lim}$	$\frac{P_u}{P_{cr.D}}$	$\frac{P_u}{P_y}$	$P_{n.D}$ (kN)	$\frac{P_y}{P_{n.D}}$	$\frac{P_u}{P_{n.D}}$
50	70	6.79	0.79	6.65	0.25	0.61	0.98	6.02	1.12	1.10
	120	11.63	1.03	9.83	1.34	0.90	0.85	8.50	1.37	1.16
	250	24.23	1.49	15.83	17.11	1.45	0.65	12.68	1.92	1.25
	300	29.08	1.63	18.15	19.05	1.67	0.62	13.90	2.08	1.30
	350	33.93	1.76	20.27	20.92	1.86	0.60	14.99	2.27	1.35
	550	53.32	2.21	26.94	26.29	2.47	0.51	18.58	2.86	1.45
	750	72.70	2.58	31.61	29.68	2.90	0.43	21.41	3.45	1.47
	900	87.25	2.83	34.30	31.81	3.15	0.39	23.24	3.70	1.47
	1200	116.33	3.27	38.19	35.25	3.51	0.33	26.39	4.35	1.45
	1500	145.41	3.65	40.70	37.80	3.74	0.28	29.09	5.00	1.41
50(1)	120	11.84	0.95	10.82	0.71	0.83	0.91	9.23	1.28	1.18
	250	24.67	1.37	16.42	16.03	1.26	0.67	13.98	1.75	1.18
	400	39.47	1.74	22.72	22.34	1.74	0.58	17.73	2.22	1.28
	550	54.27	2.04	27.43	25.78	2.10	0.51	20.65	2.63	1.33
	750	74.01	2.38	32.11	29.01	2.45	0.43	23.85	3.13	1.35
	900	88.81	2.61	34.79	31.03	2.66	0.39	25.92	3.45	1.33
	1200	118.41	3.01	38.69	34.29	2.96	0.33	29.47	4.00	1.32
	1500	148.02	3.36	41.27	36.80	3.15	0.28	32.51	4.55	1.27
50(2)	120	12.06	0.84	11.61	0.49	0.67	0.96	10.33	1.16	1.12
	250	25.13	1.21	17.67	13.96	1.02	0.70	16.07	1.56	1.10
	400	40.21	1.52	23.64	21.05	1.37	0.59	20.59	1.96	1.15
	550	55.29	1.79	28.31	24.30	1.64	0.51	24.10	2.27	1.18
	750	75.40	2.09	33.13	28.36	1.92	0.44	27.95	2.70	1.19
	900	90.48	2.29	35.83	30.13	2.07	0.40	30.42	2.94	1.18
	1200	120.64	2.64	39.56	32.70	2.29	0.33	34.68	3.45	1.14
	1500	150.79	2.95	42.02	35.13	2.43	0.28	38.32	4.00	1.10
65	250	48.92	1.37	31.58	12.15	1.219	0.65	27.71	1.75	1.14
	300	58.71	1.50	35.69	13.92	1.377	0.61	30.44	1.92	1.18
	550	107.63	2.04	51.49	19.51	1.986	0.48	40.93	2.63	1.27
	750	146.76	2.38	60.49	22.31	2.334	0.41	47.28	3.13	1.28
	900	176.12	2.61	66.11	23.90	2.551	0.38	51.37	3.45	1.28
	1200	234.82	3.01	75.62	27.00	2.917	0.32	58.42	4.00	1.30
	1400	273.96	3.25	81.05	29.07	3.127	0.30	62.52	4.35	1.30
	1800	352.23	3.69	87.95	32.46	3.393	0.25	69.76	5.00	1.27
65(1)	150	30.03	0.91	27.78	0.87	0.770	0.92	24.16	1.25	1.15
	250	50.05	1.18	36.05	7.43	1.000	0.72	32.67	1.54	1.10
	550	110.10	1.75	53.98	19.69	1.497	0.49	49.14	2.22	1.10
	750	150.14	2.04	63.06	22.33	1.749	0.42	57.02	2.63	1.11
	900	180.17	2.24	68.79	24.13	1.908	0.38	62.09	2.94	1.11
	1200	240.22	2.58	78.35	27.21	2.173	0.33	70.82	3.45	1.11
	1400	280.26	2.79	83.74	29.43	2.322	0.30	75.91	3.70	1.10
	1800	360.33	3.16	90.08	32.21	2.498	0.25	84.86	4.17	1.06

Table A2: Numerical distortional failure loads and DSM estimates for the SLC 65(2)-65(3)-75-75(1)-80 columns analyzed.

SLC	f_y (MPa)	P_y (kN)	λ_D	P_u (kN)	$(\lvert\delta\rvert/t)_{\lim}$	$\frac{P_u}{P_{cr.D}}$	$\frac{P_u}{P_y}$	$P_{n.D}$ (kN)	$\frac{P_y}{P_{n.D}}$	$\frac{P_u}{P_{n.D}}$
65(2)	150	30.30	0.85	28.85	0.44	0.69	0.95	25.59	1.19	1.12
	250	50.50	1.10	38.48	6.98	0.92	0.76	34.99	1.45	1.10
	550	111.09	1.63	55.31	18.31	1.33	0.50	53.15	2.08	1.04
	750	151.49	1.91	64.19	21.81	1.54	0.42	61.81	2.44	1.04
	900	181.79	2.09	69.86	23.65	1.67	0.38	67.39	2.70	1.04
	1200	242.38	2.41	79.56	26.96	1.91	0.33	76.99	3.13	1.03
	1400	282.78	2.60	84.85	29.13	2.03	0.30	82.57	3.45	1.03
	1800	363.57	2.95	91.27	32.12	2.19	0.25	92.41	4.00	0.99
65(3)	100	19.45	0.89	18.23	0.54	0.74	0.94	15.93	1.22	1.15
	150	29.17	1.09	22.92	4.82	0.93	0.79	20.37	1.43	1.12
	250	48.62	1.41	31.83	11.34	1.30	0.65	26.91	1.82	1.18
	400	77.79	1.78	43.75	14.97	1.78	0.56	34.06	2.27	1.28
	550	106.96	2.09	52.79	17.59	2.15	0.49	39.65	2.70	1.33
	750	145.86	2.44	62.16	20.01	2.53	0.43	45.76	3.23	1.35
	900	175.03	2.67	67.72	21.70	2.76	0.39	49.70	3.57	1.37
	1200	233.37	3.08	76.86	23.97	3.13	0.33	56.50	4.17	1.35
75	100	30.47	0.74	29.78	0.36	0.53	0.98	28.06	1.09	1.06
	250	76.17	1.17	56.00	6.24	1.00	0.74	50.09	1.52	1.12
	350	106.64	1.38	68.30	11.18	1.22	0.64	60.05	1.79	1.14
	550	167.58	1.73	90.09	15.64	1.61	0.54	75.43	2.22	1.19
	750	228.52	2.02	106.67	17.54	1.91	0.47	87.55	2.63	1.22
	900	274.22	2.22	116.74	19.35	2.09	0.43	95.35	2.86	1.22
	1200	365.63	2.56	133.41	21.54	2.39	0.36	108.78	3.33	1.22
	1700	517.98	3.05	155.16	25.28	2.78	0.30	127.12	4.00	1.22
75(1)	200	92.96	0.69	91.56	0.25	0.47	0.98	88.47	1.05	1.03
	300	139.44	0.85	132.84	0.34	0.68	0.95	118.41	1.18	1.12
	480	223.10	1.07	179.38	3.46	0.92	0.80	158.37	1.41	1.14
	650	302.12	1.24	216.84	5.53	1.11	0.72	187.71	1.61	1.15
	850	395.07	1.42	259.87	7.38	1.33	0.66	216.37	1.82	1.20
	950	441.55	1.50	279.98	8.08	1.43	0.63	229.08	1.92	1.22
	1200	557.75	1.69	325.40	9.42	1.67	0.58	257.46	2.17	1.27
	1800	836.63	2.07	412.50	11.73	2.11	0.49	312.84	2.70	1.32
	2200	1022.55	2.29	456.93	12.89	2.34	0.45	343.47	2.94	1.33
	2800	1301.42	2.58	506.99	14.19	2.60	0.39	383.44	3.45	1.32
	3500	1626.78	2.89	547.43	15.64	2.81	0.34	423.82	3.85	1.30
80	250	138.21	0.72	131.53	0.49	0.49	0.95	129.08	1.08	1.02
	550	304.07	1.07	227.23	4.03	0.85	0.75	216.36	1.41	1.05
	750	414.64	1.25	256.06	5.45	0.96	0.62	257.47	1.61	0.99
	1200	663.42	1.58	307.42	9.79	1.15	0.46	328.89	2.00	0.93
	1800	995.14	1.93	369.20	12.47	1.38	0.37	400.96	2.50	0.92
	2200	1216.28	2.13	403.13	13.95	1.51	0.33	440.79	2.78	0.92
	3000	1658.56	2.49	452.92	16.29	1.69	0.27	508.50	3.23	0.89
	3500	1934.98	2.69	475.86	17.57	1.78	0.25	545.20	3.57	0.87

Table A3: Numerical distortional failure loads and DSM estimates for the SLC 90-90(1)-90(2)-90(3)-100 columns analyzed.

SLC	f_y (MPa)	P_y (kN)	λ_D	P_u (kN)	$(\lvert\delta\rvert/t)_{\text{lim}}$	$\frac{P_u}{P_{cr.D}}$	$\frac{P_u}{P_y}$	$P_{n.D}$ (kN)	$\frac{P_y}{P_{n.D}}$	$\frac{P_u}{P_{n.D}}$
90	200	113.89	0.62	111.60	0.22	0.382	0.98	112.23	1.01	0.99
	550	313.20	1.04	243.03	0.50	0.833	0.78	228.25	1.37	1.06
	850	484.04	1.29	296.51	1.71	1.016	0.61	291.34	1.67	1.02
	1050	597.93	1.43	330.71	11.17	1.133	0.55	325.58	1.85	1.02
	1300	740.30	1.59	366.41	12.53	1.256	0.49	362.89	2.04	1.01
	1500	854.19	1.71	391.44	13.17	1.342	0.46	389.55	2.17	1.00
	2100	1195.87	2.02	447.57	15.04	1.534	0.37	457.98	2.63	0.98
	3500	1993.12	2.61	510.61	18.73	1.750	0.26	579.62	3.45	0.88
90(1)	250	137.87	0.92	123.02	0.53	0.75	0.89	110.56	1.25	1.11
	400	220.58	1.16	162.82	5.996	0.99	0.74	146.01	1.52	1.11
	550	303.30	1.36	203.81	8.399	1.24	0.67	173.48	1.75	1.18
	750	413.60	1.59	251.76	10.632	1.53	0.61	203.37	2.04	1.23
	1000	551.46	1.83	299.44	12.335	1.83	0.54	234.23	2.38	1.28
	1200	661.75	2.01	330.64	13.293	2.02	0.50	255.54	2.56	1.30
	1450	799.62	2.21	363.11	14.523	2.21	0.45	279.23	2.86	1.30
	1900	1047.78	2.53	409.57	16.023	2.50	0.39	316.09	3.33	1.30
90(2)	250	135.62	1.08	107.55	2.15	0.92	0.79	95.79	1.41	1.12
	400	216.98	1.36	148.23	8.937	1.26	0.68	124.04	1.75	1.19
	550	298.35	1.60	186.82	12.079	1.59	0.63	146.01	2.04	1.28
	850	461.09	1.98	249.19	15.526	2.13	0.54	180.43	2.56	1.39
	1000	542.46	2.15	273.75	16.596	2.34	0.50	194.76	2.78	1.41
	1200	650.95	2.36	300.93	18.120	2.57	0.46	211.90	3.03	1.43
	1450	786.57	2.59	328.57	19.579	2.80	0.42	230.97	3.45	1.43
	1850	1003.55	2.93	362.81	21.429	3.10	0.36	257.61	3.85	1.41
90(3)	300	168.14	1.03	139.85	1.19	0.88	0.83	123.15	1.37	1.14
	450	252.21	1.26	175.86	9.095	1.11	0.70	154.79	1.64	1.14
	650	364.30	1.52	221.78	12.746	1.40	0.61	187.61	1.96	1.18
	850	476.39	1.73	260.43	14.891	1.64	0.55	214.41	2.22	1.22
	1100	616.51	1.97	299.07	16.854	1.89	0.49	242.76	2.56	1.23
	1300	728.60	2.14	323.80	18.203	2.04	0.44	262.62	2.78	1.23
	1500	840.69	2.30	344.36	19.012	2.17	0.41	280.64	3.03	1.23
	2000	1120.92	2.66	383.89	21.461	2.42	0.34	319.91	3.45	1.20
100	150	59.16	1.29	41.27	9.64	1.17	0.70	35.45	1.67	1.16
	250	98.59	1.67	59.94	14.672	1.70	0.61	46.07	2.13	1.30
	350	138.03	1.98	74.93	18.035	2.12	0.54	54.21	2.56	1.39
	440	173.52	2.22	85.62	19.674	2.42	0.49	60.35	2.86	1.43
	550	216.90	2.48	96.39	21.486	2.73	0.44	66.87	3.23	1.45
	750	295.78	2.89	111.94	24.132	3.17	0.38	76.88	3.85	1.45
	1000	394.37	3.34	126.90	26.771	3.59	0.32	87.29	4.55	1.45
	1200	473.24	3.66	136.28	28.843	3.86	0.29	94.50	5.00	1.45

Table A4: Numerical distortional failure loads and DSM estimates for the SLC 100(1)-120-150-120(1)-120(2)-120(3)-140-140(1) columns analyzed.

SLC	f_y (MPa)	P_y (kN)	λ_D	P_u (kN)	$(\lvert\delta\rvert/t)_{\mathrm{lim}}$	$\frac{P_u}{P_{cr.D}}$	$\frac{P_u}{P_y}$	$P_{n.D}$ (kN)	$\frac{P_y}{P_{n.D}}$	$\frac{P_u}{P_{n.D}}$
100(1)	250	179.56	1.04	147.65	1.39	0.90	0.82	130.05	1.39	1.14
	350	251.39	1.24	181.95	6.32	1.10	0.72	157.25	1.59	1.16
	450	323.22	1.40	218.56	8.52	1.33	0.68	179.74	1.79	1.22
	550	395.04	1.55	253.28	10.19	1.54	0.64	199.19	2.00	1.27
	750	538.69	1.81	314.48	12.54	1.91	0.58	232.15	2.33	1.35
	1000	718.26	2.09	374.67	14.74	2.27	0.52	266.24	2.70	1.41
	1200	861.91	2.29	413.89	15.79	2.51	0.48	289.81	2.94	1.43
	1700	1221.04	2.72	485.53	18.37	2.95	0.40	339.55	3.57	1.43
120	120	63.87	0.67	63.25	0.32	0.44	0.99	61.62	1.04	1.03
	250	133.07	0.96	121.20	0.59	0.85	0.91	102.79	1.30	1.18
	350	186.30	1.14	135.82	2.18	0.95	0.73	125.21	1.49	1.09
	550	292.75	1.43	166.57	17.41	1.16	0.57	159.71	1.82	1.04
	750	399.21	1.67	194.07	22.08	1.35	0.49	186.78	2.13	1.04
	900	479.05	1.83	210.64	24.54	1.47	0.44	204.17	2.33	1.03
	1200	638.74	2.11	235.25	28.55	1.64	0.37	234.08	2.70	1.00
	1800	958.10	2.58	261.97	33.82	1.83	0.27	282.05	3.45	0.93
150	120	138.63	0.88	132.53	0.38	0.74	0.96	114.33	0.82	0.86
	200	231.05	1.14	175.17	6.63	0.98	0.76	155.43	0.67	0.89
	250	288.81	1.27	204.78	9.32	1.15	0.71	175.73	0.61	0.86
	350	404.33	1.51	263.22	13.16	1.48	0.65	209.51	0.52	0.80
	550	635.38	1.89	361.61	17.61	2.03	0.57	261.80	0.41	0.72
	750	866.43	2.20	435.17	20.33	2.44	0.50	303.02	0.35	0.70
	900	1039.72	2.42	478.64	21.93	2.69	0.46	329.57	0.32	0.69
	1200	1386.29	2.79	545.12	24.54	3.06	0.39	375.33	0.27	0.69
	1500	1732.86	3.12	592.44	26.64	3.32	0.34	414.42	0.24	0.70
120(1)	285	160.96	1.48	101.91	17.79	1.39	0.63	84.61	1.89	1.20
120(2)	284	166.03	1.72	100.60	18.71	1.79	0.61	75.30	2.22	1.33
120(3)	283	174.01	1.81	104.37	20.00	1.96	0.60	74.99	2.33	1.39
140	285	176.72	1.62	106.13	18.38	1.57	0.60	85.25	2.08	1.25
140(1)	285	181.69	1.92	105.45	19.65	2.14	0.58	73.54	2.50	1.43

APPENDIX B

Data concerning PLC columns[15]

Table B1 provides, for each PLC columns reported in the literature and characterized in Tables 3.2 , the f_y (yield stress), P_y (squash load), λ_D (distortional slenderness), P_u (failure load) and $P_u/P_{n.D}$ (numerical-to-predicted failure load ratio) values.

[15] By LANDESMANN & CAMOTIM (2013) or SANTOS *et. al.* (2014).

Table B1: Numerical distortional failure loads and DSM estimates for the PLC columns reported.

PLC	f_y (MPa)	P_y (kN)	λ_D	P_u (kN)	$\frac{P_u}{P_{n.D}}$
60	250	100.0	0.64	98.80	1.01
	550	220.0	0.94	186.00	1.08
	700	280.0	1.06	210.90	1.04
	1200	480.0	1.39	293.50	1.09
75	250	122.5	0.76	115.50	1.03
	550	269.5	1.13	188.60	1.03
	700	343.0	1.27	218.60	1.04
85	345	309.5	1.19	206.07	1.03
85(1)	345	242.9	0.86	212.29	1.04
110	250	187.5	0.67	185.20	1.03
	550	412.5	0.99	346.50	1.11
	700	525.0	1.12	397.90	1.11
100	345	283.9	1.02	219.48	1.05
100(1)	345	362.3	1.40	213.97	1.06
100(2)	345	229.1	0.79	214.62	1.05
130	345	366.4	1.35	228.18	1.08
130(1)	345	468.2	1.89	227.02	1.18
130(2)	345	295.0	1.01	231.45	1.05
150	345	338.8	1.17	231.99	1.04
150(1)	345	421.3	1.55	231.01	1.09
150(2)	345	538.6	2.17	231.51	1.20
180	345	404.7	1.40	229.53	1.02
180(1)	345	503.4	1.90	230.25	1.11
180(2)	345	644.5	2.62	232.93	1.25
200	345	448.5	1.56	229.66	1.02
200(1)	345	627.2	2.24	260.09	1.20
200(2)	345	714.8	2.97	234.14	1.30